Reduction of translating ribosomes enables *Escherichia coli* to maintain elongation rates during slow growth

Dai X, et al

Supplementary Information

Table of Contents

Supplementary Notes

Supplementary Note 1: Growth law and the translational elongation rate for nutrient-limited growth.

In this study, we characterized the growth-rate dependence of ribosome content (RNA/protein ratio) and the *in vivo* translational elongation rate, under a very broad range of nutrient conditions (Fig. 1A-D). This allows us to reexamine critically several historical issues regarding the apparent contradiction between the linear growth law, attributed originally to a constant translational elongation rate[1], and the observed growth-rate dependence of the elongation rate. The results give us important insights into the different forces governing protein synthesis across different growth conditions, as discussed in detail in this Note.

A. The linear growth law and its historical interpretation.

Starting from the late 1950s, a series of quantitative studies on the macromolecular composition were carried out for cells growing exponentially in batch culture[2-4]. We will describe the outcome of such studies using more recent notation: All extensive quantities refer to batch culture measurements taken over some "standard culture volume", e.g., 1 ml of culture normalized to a density of $OD_{600}=1$. The total RNA and protein mass in a standard culture volume is denoted by R and P, respectively, and the total number of ribosomes is N_{Rb}.

The cellular RNA-protein ratio ($r \equiv R/P$) is known to depend linearly on the growth rate (λ) for nutrient-limited growth over a range of moderate to fast growth [2,5,6]. This relation is referred to as a bacterial growth law. In Scott et al[6], this relation was expressed as

$$ r = r_0 + \lambda/\kappa_t \,, \qquad\qquad [N1.1] $$

where r_0 is the vertical intercept, and κ_t is the inverse of the slope. The latter is called "translation capacity" because it was shown to be linearly proportional to the *in vitro* translational elongation rate[6].

The RNA-protein ratio is a proxy of the ribosome abundance because most of the total RNA is ribosomal RNA. It is useful to express the RNA/protein ratio in term of the abundance of ribosomes. The total mass of rRNA in this culture is $M_{rRNA} = N_{Rb} \cdot m_{rRNA}$, where m_{rRNA} is the mass of rRNA in a single ribosome[1]. Since ~86% of total RNA is rRNA in exponentially growing cells[2,5] (data plotted in Supplementary Fig. 15), the ribosome content is linked to the total RNA

---

[1] Each ribosome contains 4566 nucleotides (5S, 16S and 23S rRNA). The average molecular weight of a nucleotide is 324. Thus $m_{rRNA} = 4,566 \times 324 = 1,479,384$.

abundance as

$$N_{Rb} = 0.86R/m_{rRNA} \qquad\qquad [N1.2]$$

The total mass of ribosomal proteins is $M_{Rb} = N_{Rb} \cdot m_{Rb}$, where $m_{Rb} = 806{,}960$ is the mass of ribosomal proteins in a single ribosome[b]. Thus the mass fraction of ribosomal proteins among all cellular proteins P, $\phi_{Rb} \equiv M_{Rb}/P$ (Referred to as the 'proteome fraction' of ribosomes or the "ribosomal fraction"), is related to the RNA-protein ratio as $r = \sigma \cdot \phi_{Rb}$, where $\sigma = m_{rRNA}/(0.86 \times m_{Rb}) \approx 2.1$. Then Eq. [N1.1] can be rewritten as

$$\phi_{Rb} = \phi_{Rb,0} + \lambda/\kappa_t' \ , \qquad\qquad [N1.3]$$

where $\phi_{Rb,0} = r_0/\sigma$ and $\kappa_t' = \kappa_t \cdot \sigma$. [We estimated ϕ_{Rb} by adding up the absolute abundance of ribosomal proteins as determined by quantitative mass spectroscopy for the growth conditions used in this study (Supplementary Table 8-10). The result is plotted against the RNA/protein ratio obtained for the same growth conditions. A linear relation is seen with slope = 2.4 and linearity coefficient = 0.98. The small discrepancy between the obtained slope and the value of σ given above Eq. [N1.3] should be attributed to the incomplete detection of certain ribosomal proteins (Supplementary Table 9)

The linear relation [N1.1] or [N1.3] is commonly and most conveniently attributed to a constant translational elongation rate[1,6]. Consider the existence of two classes of ribosomes, those that are active and translate at the same rate k (in aa/s), and those not engaged in translation at all. Let the abundance of the active ribosomes be N_{Rb}^{active} per volume of standard culture. Then the total rate of protein synthesis is $k \cdot N_{Rb}^{active}$, measured in the number of amino acid (aa) residues. On the other hand, the rate of total protein accumulation[c] in an exponentially growing culture[7] is $\lambda \cdot P/m_{aa}$, measured in the number of aa residues contained in all proteins, with $m_{aa} \approx 110$. Equating these two quantities, we obtain

$$k \cdot N_{Rb}^{active} = \lambda \cdot P/m_{aa}. \qquad\qquad [N1.4]$$

We note that the ratio of Eqs. [N1.2] and [N1.4] defines the fraction of active ribosome equivalent,

$$f_{active} \equiv \frac{N_{Rb}^{active}}{N_{Rb}} = \frac{\lambda \cdot \sigma'}{k \cdot (R/P)} \ , \qquad\qquad [N1.5]$$

where $\sigma' \equiv m_{rRNA}/(0.86 m_{aa}) \approx 1.56 \times 10^4$ is a dimensionless constant. The fraction of active ribosome equivalent, f_{acitve} can therefore be calculated based on the values of R/P, λ, and k listed in Supplementary Table 1-5 and 11-12 for each growth condition[d].

---

[b] The ribosomal proteins contain a total of $n_{Rb} = 7336$ amino acid residues, with average MW of $m_{aa} = 110$[6].

[c] This assumes that the average protein turnover rate is negligible, which is approximately true for exponentially growing *E. coli* cells[7].

[d] Note that for Cm-inhibited cells, while R/P is still a good proxy of total r-protein abundances as

3

Defining $\phi_{Rb}^{active} \equiv N_{Rb}^{active} \cdot m_{Rb}/P$, the mass-balance equation [N1.4] can be alternatively expressed as $\phi_{Rb}^{active} = \lambda/\gamma$, where $\gamma \equiv k/n_{Rb}$ is the translational elongation rate in the special unit of n_{Rb}, the number of aa residues in a ribosome; i.e., $1/\gamma$ is the time it take for one active ribosome to synthesize all the proteins in a ribosome. Alternatively, this relation can be written as

$$\phi_{Rb} = \phi_{Rb}^{inact} + \lambda/\gamma, \qquad\qquad [\text{N1.6}]$$

where $\phi_{Rb}^{inact} \equiv \phi_{Rb} - \phi_{Rb}^{active}$ is the proteome fraction of inactive ribosomes.

Comparison of Eq. [N1.3] with Eq. [N1.6] shows that the simplest rationalization of the linear growth law is to interpret $\phi_{Rb,0}$ as the proteome fraction of inactive ribosomes, i.e., $\phi_{Rb,0} = \phi_{Rb}^{inact}$. Then the empirical parameter κ'_t is identified with γ, i.e., the translational elongation rate in suitable unit. This identification is supported by the empirical observation that κ_t (hence κ'_t) is linearly proportional to the *in vitro* translational elongation rate[6].

B. Klumpp et al's reconciliation of the historical interpretation.

The above historical interpretation contradicts the observed growth-rate dependent translational elongation rate, which was known already since the mid-1970s (Supplementary Fig. 5). To reconcile the contradiction, Klumpp et al[8] developed a coarse-grained theory of proteome partitioning based on the co-regulation between ribosome and the tRNA-affiliated proteins, and the limitation of tRNA diffusion due to macromolecular crowding. This theory is referred to here as the "crowding theory".

In the crowding theory[8], Klumpp et al took the mass-balance relation Eq. [N1.4] as a starting point[e], allowing the elongation rate γ (proportional to k) to be variable. They explicitly incorporated the translation-affiliated proteins (EF-Tu, EF-G, EF-Ts, tRNA synthetases, etc) into their model. They assumed that the proteome fraction of these proteins, ϕ_T, is proportional to the ribosomal fraction, i.e.,

$$\phi_T = \alpha \cdot \phi_{Rb} \quad , \qquad\qquad [\text{N1.7}]$$

since many affiliated translational proteins are known to be co-regulated with the ribosomes, and deduced a proportionality constant $\alpha \approx 0.6$ based on existing empirical data (see, e.g., Supplementary Fig. 13B).

---

shown in Supplementary Fig. 8, the latter no longer bears a simple relation with the number of ribosomes, N_{Rb}, which becomes difficult to define due to premature precursors resulting from ribosome mis-assembly[9] (Supplementary Fig. 12). In this study, we will use the total r-protein abundance to estimate ϕ_{Rb} even for Cm-treated cells. This effectively amounts to including the misassembled ribosomal precursors as "inactive" ribosomes given our definitions of active and inactive ribosomes.

[e] Note that in Klumpp et al's notation, they used $\phi_{Rb,0}$ to refer to ϕ_{Rb}^{inact}

Since ϕ_T mainly consists of components of charged tRNA ternary complex, the model assumes that the elongation rate exhibits a Michaelis-Menten dependence on ϕ_T, i.e.,

$$\gamma = \gamma_{\max} \cdot \frac{\phi_T}{\phi_T + \varphi_M}, \qquad\qquad [\text{N1.8}]$$

where $\gamma_{\max} \equiv k_{elong}/n_{Rb}$, φ_M being the Michaelis constant for ϕ_T, i.e., the value of ϕ_T where the elongation rate γ drops to half of its maximal value, $\gamma_{\max}$.

In a simplifying analysis where $\phi_T \propto \lambda$, Eq. [N1.8] becomes

$$\gamma = \gamma_{\max} \cdot \frac{\lambda}{\lambda + \lambda_M}, \qquad\qquad [\text{N1.9}]$$

which suggests that the elongation rate also has a Michaelis-Menten relation with the growth rate λ. Inserting Eq. [N1.9] back to Eq. [N1.6] yields:

$$\phi_{Rb} = \frac{\lambda}{\gamma_{max}} + \phi_{Rb}^{inact} + \lambda_M/\gamma_{max}. \qquad\qquad [\text{N1.10}]$$

Eq. [N1.10] provides a unique interpretation of the empirical growth law (Eq. [N1.3]), that the slope of the linear relation between ribosome content and growth rate (i.e., the parameter γ in Eq. [N1.6]) corresponds to the inverse of γ_{max} or k_{elong}, and that the constant offset $\phi_{Rb,0}$ has a contribution from the inactive ribosomes (ϕ_{Rb}^{inact}) which is assumed to be constant, as well as a contribution from the binding properties of the ternary complexes.

The above simplifying analysis reveals a way to reconcile the apparent contradiction between the growth-rate dependent translational elongation rate and the linear correlation between the ribosome content and growth rate. The crowding theory suggests that the historical interpretation is conceptually correct, erring only in the identification of phenomenological parameters to specific molecular processes. Most importantly, the slope of the linear relation between the ribosome content and growth rate is determined by the maximal rate of elongation, not the actual elongation rate in a given growth condition. Consequently, there is no contradiction between the linear growth law and the growth-rate dependence of the elongation rate.

However, the full solution of the crowding theory predicts that the ribosomal content ϕ_{Rb} and the elongation rate drops to zero as the growth rate approaches zero (Fig. 3A & 3B of Ref. [8]). This result does not make physiological sense, as timely protein expression is desirable for cells even in stationary phase. The resolution to this conundrum, based on the data generated by this study, is described in Supplementary Note 4.

5

Supplementary Note 2: Effect of antibiotics on translational elongation.

To understand the effect of Chloramphenicol (Cm) inhibition on the measured translational elongation rate, we need to know two things: First, what is the probability that a translating ribosome is hit by Cm during translation of LacZ? Secondly, because our method only measures the translational elongation rate of complete proteins (and not aborted polypeptides), we additionally need to know the probability that the affected ribosome will eventually complete translation. In the following, we will perform the analysis for the highest Cm concentration of 8 μM used in our experimental study.

In the first case, we note that the frequency of Cm binding to a single ribosome is

$$k_{\text{hit}} = k_{\text{on}}[\text{Cm}]_f \qquad\qquad [\text{N2.1}]$$

where k_{on} is the binding constant, measured to be 0.034 $(\mu\text{M·min})^{-1}$ [9], and $[\text{Cm}]_f$ is the concentration of free (unbound) Cm in the cytosol. The probability of being hit at least once by a Cm during translation is then

$$P_{\text{hit}} = 1 - \exp(-k_{\text{hit}}\tau_{X0}) \qquad\qquad [\text{N2.2}]$$

where τ_{X0} is the time for translation in the absence of Cm, about 72 s for saturating concentrations of tRNA (Supplementary Fig. 2). To a first approximation, we can assume that chloramphenicol is in diffusive equilibrium across the cell membrane. This means that the free concentration of chloramphenicol in the cytosol is equal to the concentration in the external medium: $[\text{Cm}]_f = [\text{Cm}] \sim 8$ uM. The concentration of chloramphenicol bound to the ribosomes is then determined by the equilibrium rate equations:

$$[\text{Cm}]_f + [R]_f \leftrightarrow [\text{Cm} \cdot R]$$

$$\frac{k_{\text{on}}}{k_{\text{off}}} = \frac{[R \cdot \text{Cm}]}{[R]_f[\text{Cm}]_f}$$

$$[R \cdot \text{Cm}] = [\text{Cm}] - [\text{Cm}]_f \qquad\qquad [\text{N2.3}]$$

where $[R]_f$ is the concentration of ribosomes not in complex with Cm, (and excluding immature ribosomes and ribosomes in the 30S and 50S subunits), and $[R]_{tot}$ is the total ribosome concentration.

With k_{off} = 0.084/min is the rate of dissociation[9], we can solve Eq. [N2.1]-[N2.3] for the free ribosome concentration:

$$\frac{[R]_f}{[R]_{tot}} = \frac{k_{off}}{k_{on}}\left([Cm] + \frac{k_{off}}{k_{on}}\right)^{-1} \qquad\qquad [\text{N2.4}]$$

We plot this relationship with our data in Figure N1 and see that it agrees well with the f_{active} decrease upon with Cm treatment. This indicates that binding of Cm to ribosome can largely account for the decrease of active ribosome fraction upon Cm inhibition.
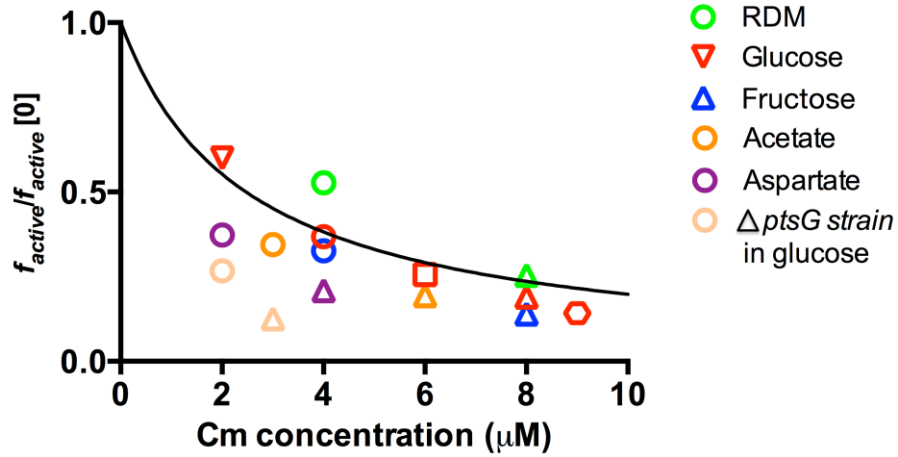
Fig. N1 Comparison between the fractions of ribosomes not in complex with Cm ($[R]_f$) in total ribosome ($[R]_{tot}$) with the f_{active} decrease in various growth conditions. The black line shows the correlation as predicted by Eq. [N2.4], denotes the change of $\frac{[R]_f}{[R]_{tot}}$ in different Cm concentration. The symbols show the relative change of f_{active} of different Cm concentration in different nutrient conditions, as represented by $f_{active}/f_{active}[0]$, where $f_{active}[0]$ is the f_{active} value in conditions without Cm.

Perhaps surprisingly then, the probability that a ribosome is hit during passage along the RNA is only $P_{hit} = 27.85\%$; that is, 72% of ribosomes translate the entire message without being impacted by the drug, even at the highest Cm concentration used. These ribosomes explain why the measured translation rate in our experiments was seemingly unaffected by the antibiotic treatment. Additionally, because the half-life of the Cm bound complex is 8.25 minutes, not only the affected ribosome, but also all downstream ribosomes will be prevented from translating; see Supplementary Fig. 12. This secondary effect of Cm due to the stalling of the lead translating ribosome could further reduce the protein synthesis rate, especially for highly translated proteins.

To find how much the stalled ribosomes contribute to complete protein product, we need to calculate how many of the stalled ribosomes recover and eventually finish translating before the mRNA is degraded. Because the stalled ribosome will leave large parts of the mRNA unprotected by ribosomes (newly synthesized part of RNA polymerase) as depicted in Supplementary Fig. 12, we expect that the mRNA degradation rate will be increased from the typical values known for WT cells grown in the absence of Cm. However, we can get an upper bound on the number of complete translations by assuming mRNA is degraded at the typical rate of $k_d = 0.46$/min (half-life of 90s)[10]. The probability that the mRNA will be degraded within the stall time t_s is

$$P_d(t_s) = 1 - \exp(-k_d t_s) \ . \tag{N2.5}$$

To find the survival probability of the stalled ribosomes P_s, we need to integrate this over the

distribution of stall times $p(t_s) = k_{\text{off}}\exp(-k_{\text{off}}t_s)$:

$$P_s = 1 - \int_0^\infty p(t_s)P_d(t_s)\,dt_s = \frac{k_{\text{off}}}{k_d + k_{\text{off}}}\ . \qquad\qquad \text{[N2.6]}$$

From Eq. [N2.6], we find that a stalled ribosome will complete translation with a probability of 15%.

Putting Eq. [N2.2] and Eq. [2.6] together gives an upper bound for the fraction of full-length proteins that will exhibit a lower average elongation rate: $F_{\text{slow}} = P_{\text{hit}} \cdot P_s \approx 4\%$. In reality, F_{slow} may be much lower than this since cells may quickly abort Cm-stalled ribosome instead of waiting for Cm to be released and translation resumed, in order to prevent the lethal effect of stalled ribosomes accumulation. But even with $F_{\text{slow}} \approx 4\%$, translation slow down by such a small number of proteins would not show up in our elongation rate measurement (even for the highest Cm concentration considered here), thereby explaining why the measured elongation rate is not lowered by the action of Cm.

We can repeat this analysis for cells grown in fusidic acid (FA), where our measurements do reveal a slowdown in elongation rate. The binding and dissociation constants have not been measured for FA; however, *in vitro* experiments suggest both a higher k_{on} and k_{off} for fusidic acid [11]. It has been shown that erythromycin (similar to chloramphenicol in our measurements) effectively stops translation at certain codons, which is what we would expect to see since its dissociation constant (k_{off}, 0.15/min) is also very low as for Cm[12]. Alternatively, the codon transit time is more uniformly increased under FA, which could result from rapid binding and unbinding of FA from EF-G-GDP on the ribosome. In this case, the number of binding events during translation is

$$N_{\text{hit}} = k_{\text{hit}}\tau_{X0} \gg 1. \qquad\qquad \text{[N2.7]}$$

The distribution of delay times can be regarded as Gaussian, and the average elongation rate can be obtained as

$$\tau_X = \tau_{X0} + \frac{N_{\text{hit}}}{k_{\text{off}}}\ . \qquad\qquad \text{[N2.8]}$$

If N_{hit} is roughly proportional to the concentration of FA, then we expect the elongation rate to decrease linearly with [*FA*], which is what we observe (Supplementary Fig. 13C). Additionally, for fast k_{on} and k_{off}, we expect the ribosomal coverage of mRNA to remain high until the elongation rate becomes lower than the innate RNAP velocity.

Supplementary Note 3: Translational elongation and ribosomal content.

A. Ternary Complexes

The Michaelis-Menten relation between the translational elongation rate (ER, denoted by k) and the ribosomal content (RNA-Protein ratio, or R/P) described in Eq. [1] of the main text depends critically on the proportionality between the concentration of ternary complexes (TC), [TC], and R/P. To justify this claim, and to compute the constant of proportionality C (in Eq. [2] of the main text), we spell out the relationship between [TC] and R/P in detail,

$$[TC] \equiv \frac{N_{TC}}{W} = \left(\frac{N_{TC}}{P}\right)\left(\frac{P}{W}\right). \qquad [N3.1]$$

Here, N_{TC} is the number of TC per standard culture volume, and P, W refers to the mass of total protein and cytoplasmic water per standard culture volume, respectively. P/W is the mass of total protein per cytoplasmic water volume.

The proportionality between [TC] and R/P is derived from the fact that a) the mass fraction of TC is approximately proportional to R/P, and b) the ratio of total protein to cytoplasmic water (P/W) is approximately constant, for growth under either nutrient limitation or Cm inhibition. The details are explained below.

a) Proportionality of ternary complex and ribosome abundances:

Each ternary complex is comprised of one charged-tRNA and one EF-Tu. Below we address each of the three components: i) tRNA abundance, ii) tRNA charging, and iii) EF-Tu abundance.

i. Previous reports showed that the ratio of rRNA to total RNA was ~86% for growth under both nutrient limitation and Cm inhibition (orange and green symbols in Supplementary Fig. 15A, respectively, for data described in Bremer & Dennis[22] and Harvey et al[5,9]). Since tRNA is by far the next most abundant RNA species to rRNA, the constant ratio of rRNA: total RNA suggests that tRNA-rRNA ratio is also constant. While direct data for tRNA abundance under Cm inhibition is not available, the proportionality of the abundance of tRNA and rRNA under nutrient limitation is directly verified in Supplementary Fig. 15B (based on the data of Bremer & Dennis[5]), giving ~ 9 tRNA/ribosome.

ii. Since TC involves the charged fraction of tRNA (aa-tRNA), we additionally measured the charging ratio of a number of tRNA species by Northern blot[13]. We find that the charging ratios remain nearly constant at approximately 75% under all conditions investigated (Supplementary Fig. 17). Thus the ratio of charged tRNA to ribosomes should also be constant, given by $75\% \times 9 \approx 7$ charged tRNA/ribosome.

iii. The abundance of EF-Tu is available from a recent quantitative proteomic study[14]. The

ratio of the mass of EF-Tu to total protein mass is shown to depend linearly on the RNA-protein ratio, under both nutrient limitation and Cm inhibition (Supplementary Fig. 14A, B). Using the MW of EF-Tu, $m_{Tu} = 4.3 \times 10^4$, we obtain the following ratio between the number of EF-Tu (N_{Tu}) and the amount of RNA (R) per standard culture volume:

$$N_{Tu}/R \approx 3.5 \times 10^{-6} \ , \qquad\qquad\qquad \text{[N3.2]}$$

Further using Eq. [N1.2] to convert the RNA abundance to number of ribosomes, we obtain ~6.1 EF-Tu/ribosome.

From the above analysis, we see that the components of TC are all nearly constant under our growth conditions. To estimate the abundance of TC, we note that the abundance of EF-Tu (~6.1/ribosome) is slightly below that of charged tRNA (~7/ribosome). We thus take the abundance of EF-Tu to be the limiting factor for TC and equate the number of TC with the number of EF-Tu (18), i.e., $N_{TC} \approx N_{Tu}$. Then, Eq. [N3.1] becomes

$$[TC] \approx \frac{N_{Tu}}{W} = \left(\frac{N_{Tu}}{R}\right)\left(\frac{R}{P}\right)\left(\frac{P}{W}\right). \qquad\qquad \text{[N3.3]}$$

where N_{Tu}/R is given in Eq. [N3.2].

b) Protein-water ratio

The protein concentration is further expanded into the following expression:

$$\frac{P}{W} = \left(\frac{P}{DW}\right)\Big/\left(\frac{W}{DW}\right), \qquad\qquad \text{[N3.4]}$$

where DW indicates dry cell weight per standard culture volume. *P* and *DW* had been measured for cells grown under nutrient limitation and Cm inhibition, and were found to be $P \approx 330$ μg and $DW \approx 505$ μg (both per ml of culture at $OD_{600} = 1$), nearly independent of growth conditions[15]. The cytoplasmic water volume per dry weight was found to be $W/DW \approx 2.08$ μl/mg in glucose minimal media[16] and assumed to be independent of the medium at the same osmolarity. Putting these results together, we have

$$P/W \approx 314 \ \text{μg/μl} \ . \qquad\qquad\qquad \text{[N3.5]}$$

Together, these results indicate that R/P is a reasonable proxy for [TC], supporting the coarse-grained model of translation (Eq. [1] of the main text). To compute the constant of proportionality in Eq. [2] of the main text, we additionally need to account for the fact that it is the concentration of *individual species* of ternary complex that controls the binding rate. Below, we calculate the effective concentration of individual species$[TC_{\text{eff}}]$ from the total concentration $[TC]$.

B. Effective concentration of individual species of TC

In the spirit of the simple coarse-grained model of translation discussed by Klumpp et al[8], the average translation time per amino acid for an mRNA with N amino acids is given by

$$\langle \tau_{TR} \rangle = \frac{1}{k} = \frac{1}{N} \sum_{i=1}^{N} \left(\frac{1}{k_{elong}} + \frac{1}{k_{on}[TC_i]} \right), \qquad \text{[N3.6]}$$

where i indexes the codon position along the mRNA. k_{elong} is the forward rate constant of ribosome translocation, and k_{on} is the on-rate of binding by the cognate TC, TC_i, whose concentration is $[TC_i]$. We assume the on-rate is diffusion limited[8] so that k_{on} is not dependent on the codon itself. Further assuming the forward rate to be the same for all tRNAs, we can rewrite Eq. [N3.6] as:

$$\frac{1}{k} = \frac{1}{k_{elong}} + \frac{1}{k_{on}N} \sum_{i=1}^{N} \left(\frac{1}{[TC_i]} \right). \qquad \text{[N3.7]}$$

Next, we group the remaining sum by the codon species, c:

$$\frac{1}{k} = \frac{1}{k_{elong}} + \frac{1}{k_{on}N} \sum_{c} \left(\frac{N_c}{[TC^c]} \right), \qquad \text{[N3.8]}$$

where N_c/N is the *codon abundance* (a_c) for the cth codon, TC^c. Let the relative abundance of the cognate tRNA species be $b_c = [TC^c]/[TC]$. Then Eq. [N3.8] can be rewritten as

$$\frac{1}{k} = \frac{1}{k_{elong}} + \frac{1}{k_{on}[TC]} \sum_{c=1} \left(\frac{a_c}{b_c} \right), \qquad \text{[N3.9]}$$

The effective concentration of the individual TC species is thus obtained as

$$[TC]_{\text{eff}} \equiv \frac{[TC]}{\sum_c \left(\frac{a_c}{b_c} \right)} \approx 0.028\,[TC]. \qquad \text{[N3.10]}$$

The latter is calculated based on tRNA and codon abundance tabulated in Ref. ([17]).

Finally, from Eqs. [N3.2], [N3.3], [N3.5] and [N3.10], we derive the linear relation between R/P and $[TC]_{\text{eff}}$, i.e., Eq. [2] of the main text, with the proportionality constant C being approximately 31 μM. We can thus use the Michaelis-Menten fit of the ER vs. R/P data (Caption of Fig. 2) to obtain k_{elong} and k_{on}. Moreover, together with the R/P data shown in Supplementary Table 3, this allows us to estimate $[TC_{\text{eff}}]$ in each growth conditions upon nutrient limitation, as shown in Fig. N2.
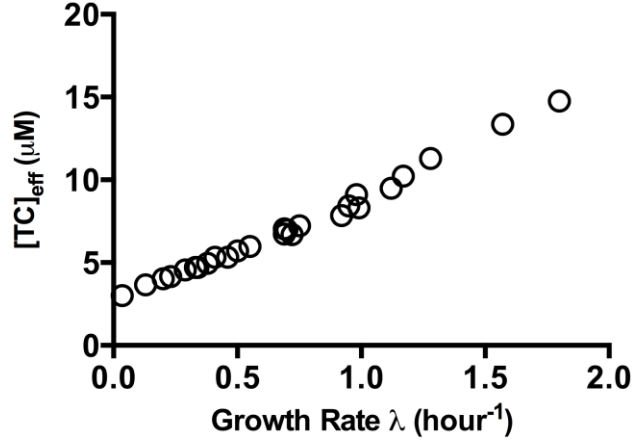
Fig. N2 $[TC_{eff}]$ **upon nutrient limitation**; Data is based on $[TC_{eff}] = C \cdot (R/P)$ with R/P data shown in Supplementary Table 3. R/P data is the average value of over three biological replicates.

C. Diffusion-limited transport of EF-G

The coarse-grained translational elongation model described above can be extended to explicitly include the translocation step facilitated by the enzyme EF-G. Because EF-G is also co-regulated with the ribosome concentration (Supplementary Fig. 14C，D), the result is a model which is functionally identical to Eq. [1] of the main text, but with a slightly modified constant, k_{on}. Mathematically, the average translation time per step is changed from Eq. [N3.6] to

$$\langle \tau_{TR} \rangle = \frac{1}{k} = \frac{1}{k_{elong}} + \frac{1}{k_{on,G}[G]} + \frac{1}{k_{on,TC}[TC_{eff}]}. \tag{N3.11}$$

Using $[G] = \beta \cdot [TC_{eff}]$ to represent the linearity between EF-G and TC concentrations, Eq. [N3.11] is reduced to the form

$$\frac{1}{k} = \frac{1}{k_{elong}} + \frac{1}{k_{on}[TC_{eff}]} \quad , \tag{N3.12}$$

where the effective on-rate, k_{on}, is given by

$$k_{on} = \frac{k_{on,TC} \cdot k_{on,G}}{k_{on,TC}/\beta + k_{on,G}} \quad . \tag{N3.13}$$

It is known that the concentration of EF-G is roughly 5 times higher than the concentration of individual species of TC[14,17]. Thus, $\beta \approx 5$. Furthermore, we expect the diffusion limited rates $k_{on,TC}$ and $k_{on,G}$ to be of similar magnitude, since EF-G and the ternary complexes are similar in physical sizes. If $k_{on,G} = k_{on,TC}$, then $k_{on} = k_{on,TC}\beta/(\beta + 1)$, which is only a 15% reduction from $k_{on,TC}$. Actually, TCs are larger due to the more rigid tRNA structure, so $k_{on,G} \gtrsim k_{on,TC}$ and k_{on} should be even better approximated by $k_{on,TC}$.

Supplementary Note 4: Reconciliation of the crowding theory with the new data.

In this study, we have characterized the *in vivo* translational elongation rate and ribosome content (RNA-protein ratio) for a wide range of growth rates for nutrient-limited growth (Fig. 1). Our data reveal discrepancy with predictions of the crowding theory by Klump et al[8] as described below.

1. Dependence of translational elongation rate on growth rate. Klumpp et al showed that the Michaelis-Menten form of the translational elongation rate $\gamma(\lambda)$ predicted by Eq. [N1.9] captured the previous data (colored symbols in Supplementary. Fig. 5). However, Eq. [N1.9] is clearly wrong given the more extensive data shown in Fig. 1A-C. Although translational elongation rate decreased at slow growth, the decrease was mild and a significant value (8-9 aa/s) was kept even close to zero growth rate. Interestingly however, despite the disagreement in the form of $\gamma(\lambda)$, a key ingredient of the crowding theory, the Michaelis-dependence of the translational elongation rate on the substrate (ternary complexes), i.e., Eq. [N1.8], is firmly established by the data (Fig. 1E. and Supplementary Fig. 15-17, which shows the linearity of TC with R/P).

2. Dependence of ribosome content on growth rate. In this work, we characterized nearly 30 growth conditions under nutrient limitation, covering a wide growth range with doubling time from 20 min to 20 hours (Supplementary Table 3). This allows us to capture the growth-rate dependence of ribosome content in detail. According to the data in Fig. 1D, ribosome content is not strictly linear with growth rate under nutrient limitation. Linearity appears to extend from the fastest growth rate down to $\sim 0.7 h^{-1}$, indicated by the dashed line in Fig. 1D. For slower growth, correlation between ribosome content and growth rate exhibits an upward bend. This is different from Klumpp et al's theory, which actually predicted a downward bend of the same plot at very slow growth (see below). This disagreement indicates a problem with the theory at slow growth.

3. Dependence of the inactive ribosome content on growth rate. One of the working assumptions of the crowding theory was a fixed (i.e., growth-rate independent) proteome fraction of inactive ribosomes. This assumption was based on Bremer's analysis of previous studies characterizing the concentration of inactive ribosomes[18]. As explained in the main text, direct characterization of inactive ribosomes is technically difficult. In this work, we have instead deduced the active (and hence also the inactive) ribosome fraction based on the measured translational elongation rate and the total ribosome fraction (Eq. [N1.5] in Supp Note 1). The results show that active ribosome fraction dramatically decreased below a growth rate of $\sim 0.5/h$ (Fig. 3C); also the absolute abundance of the inactive ribosomes, i.e., the protein mass fraction ϕ_{Rb}^{inact}, increased at slow growth (Fig. 3D).

Thus the crowding theory has multiple problems at slow growth. Of the 3 problems listed, #3 (growth-rate dependence of the abundance of inactive ribosome) is an assumption of the theory that is proven wrong by the new data, while #1 and #2 are predictions made by the theory. We

show below that the wrong predictions #1 and #2 are due only to the wrong assumption, #3.

Let us go back to the mass-balance equation, Eq. [N1.6], but express the ribosomal abundances ϕ_{Rb} and ϕ_{Rb}^{inact} in terms of the observed RNA-protein ratio, $r = R/P$ and $r_{inact} = R_{inact}/P$, respectively. Using the conversion factor $r = \sigma \cdot \phi_{Rb}$ (with σ given above Eq. [N1.3]), we can rewrite Eq. [N1.6] as

$$r(\lambda) = r_{inact}(\lambda) + \frac{\sigma' \cdot \lambda}{k(r)} \quad , \qquad\qquad \text{[N4.1]}$$

where we used $\gamma \equiv k/n_{Rb}$, with $\sigma' = \sigma \cdot n_{Rb} \approx 1.56 \times 10^4$ as given earlier (below Eq. [N1.5]). In Eq. [N4.1], we have explicitly indicated a) the growth-rate dependence of the inactive ribosome fraction via $r_{inact}(\lambda)$, and b) the dependence of the translational elongation rate k on its substrate, which is proportional to the ribosomal fraction, hence r. Note that given the mass-balance equation (Eq. [N1.4], whose validity for exponentially growing cells only depends on the stability of the majority of cellular proteins), $r_{inact}(\lambda)$ and $k(r)$ are the only two factors that can affect the dependence of the ribosome content on growth rate, $r(\lambda)$. As already stated, Klumpp et al correctly hypothesized the Michaelis-Menten form of $k(r)$, which is given by the main text (Eqs. [1] and [2]) as

$$\frac{1}{k} = \frac{1}{k_{elong}} + \frac{1}{C \cdot k_{on} r} \quad . \qquad\qquad \text{[N4.2]}$$

However, they incorrectly assumed r_{inact} to be constant (i.e., growth-rate independent). As we show below, it turns out that $r_{inact}(\lambda)$ has a more direct impact on the ribosome content $r(\lambda)$ at slow growth.

Let us combine Eqs. [N4.1] and [N4.2] into a single equation,

$$r(\lambda) = r_{inact}(\lambda) + \frac{\sigma' \cdot \lambda}{k_{elong}} \cdot \left[1 + \frac{K_M}{r(\lambda)}\right] \quad , \qquad\qquad \text{[N4.3]}$$

where $K_M = k_{elong}/(C \cdot k_{on})$. The contribution from the Michaelis dependence is the term $K_M/r(\lambda)$ in [...] of Eq. [N4.3]. Based on the fit in Fig. 2C, $K_M \approx 0.11$. The value of $r(\lambda)$ ranges from ~0.5 at the highest growth rate to ~0.25 at $\lambda \approx 0.7$/h where the upward bend of $r(\lambda)$ occurs in Fig. 1D. During this range of growth rates, the term in [...] changes from ~1.2 to ~1.5, while r_{inact} is nearly growth-rate independent (Fig. 3D). Here the system is well captured by the crowding model[8]. For slower growth rates, i.e., $0 < \lambda < 0.7$/h, $r(\lambda)$ ranges from ~0.2 to ~0.1 according to Fig. 1D; so [...] contributes a factor of 1.5~2. However, $r_{inact}(\lambda)$ rises steeply with decreasing growth rate (Fig. 3D), approximated by the expression $r_{inact}(\lambda) \approx r_{inact}(0) - b\lambda$, with the slope b being about half that of the slope σ'/k_{elong} describing the fast growth-rate range. Thus, for the slow growth-rate range, Eq. [N4.3] is dominated by $r_{inact}(\lambda)$, whose rise leads to an upward bend of $r(\lambda)$ (Fig. 1D).

To test the above reasoning, we directly solved Eq. [N4.3] which is a quadratic equation for $r(\lambda)$. First we implemented Klumpp et al's model by taking $r_{inact}(\lambda) = 0.023$ (or $\phi_{Rb}^{inact} = 1.1\%$), which corresponds to the inactive ribosome content in the high-growth range according to Fig. 3D, together with the Michaelis parameters obtained in Fig. 2C of the main text ($k_{elong} \approx 22aa/s$ and $K_M \approx 0.11$). We obtained the cyan curves in Supplementary Fig. 19A, which bends downward at small growth rates. Next, we incorporated the experimentally observed fraction of inactive ribosomes, $r_{inact}(\lambda)$, by using a smooth fit to the data in Fig. 3D. Solving for $r(\lambda)$ now yields the red curve, which captures the experimental data well without additional fitting. Predictions of the model on the translational elongation rate $k(\lambda)$, obtained by inserting the predicted form of $r(\lambda)$ plotted in Supplementary Fig. 19A into Eq. [N4.2], is shown in Supplementary Fig. 19B, again as the cyan and red curves for results without and with the growth-rate dependent forms of ϕ_{Rb}^{inact}, respectively. Thus, the crowding theory of Klumpp et al quantitatively captures the growth-rate dependence of the elongation rate and RNA-protein ratio, provided that the correct inactive ribosome fraction is supplied. This result vividly illustrates how the elongation rate can be manipulated by modulating the inactive ribosome fraction.

Supplementary Note 5: Model of abortive translation due to nutrient limitation

In the main text, we showed that the inactive ribosome fraction increased steeply for slow growing cells (poor nutrients and Cm inhibition). Two possible mechanisms were described. One was the ppGpp-mediated inhibition of translational initiation (Fig. 4A). Another was translational abortion caused by ribosome stalling (Fig. 4B). Here, we elaborate the latter mechanism further, for the case of nutrient-limited growth.

Previously, it was shown that if ribosomes stopped in the middle of translation due to the lack of an appropriate TC (e.g. under amino acid starvation or at a rare codon), translation aborted through the action of tmRNA encoded by *ssrA* rescued the stalled ribosome while tagging the nascent polypeptide for degradation[19,20]. Such stalled ribosomes thus would not produce a stable protein product, and would show up in our analysis (Supplementary Note 1) as inactive. Although this mechanism has not yet been directly reported under steady-state growth, this scenario is more likely given the slow elongation rate exhibited by nutrient-limited cells characterized in this study.

The average time a ribosome spends waiting for a TC at specific codon c is

$$\tau_{w,c} = \frac{1}{k_{on}[TC]b_c} \, , \qquad\qquad [N5.1]$$

where k_{on} is the on-rate, $[TC]$ is the total TC concentration, and b_c is the relative abundance of the cognate tRNA for codon c, as introduced in Supplementary Note 3. If we assume that binding is a Poisson process, then the distribution of waiting times t_w takes the form

$$p_c(t_w) = \frac{1}{\tau_{w,c}} e^{-t_w/\tau_{w,c}} \ , \qquad\qquad\qquad [N5.2]$$

We can find the average waiting time distribution for any codon by taking a weighted average of $p_c(t_w)$ over all of the different codons, i.e.,

$$p(t_w) = \sum_c a_c p_c(t_w) \ , \qquad\qquad\qquad [N5.3]$$

where a_c is the codon abundance in the mRNA defined in Supplementary Note 3. Note that under this formalism, the translational elongation rate is given by

$$\frac{1}{k} = \frac{1}{k_{elong}} + \int_0^\infty t_w p(t_w) dt_w \ . \qquad\qquad\qquad [N5.4]$$

The distribution $p(t_w)$ will depend on the growth rate through [TC] (or equivalently, through the RNA-protein ratio). $p(t_w)$ was calculated using the fitted value of k_{on}, and the measured codon and tRNA abundances from[17], and is shown for various values of RNA-protein ratio in Fig. N3A.

Now, if we assume that translation is aborted when the ribosome is stalled for time $t_w > t_x$, where t_x is some critical time for ssrA action to occur, then the probability that translation is aborted at a given codon is

$$P_{abort} = \int_{t_x}^\infty p(t_w) dt_w \ , \qquad\qquad\qquad [N5.5]$$

and the probability that the ribosome will make it all the way to the end of a message of length N without being aborted is approximately

$$P_s = (1 - P_{abort})^N \ . \qquad\qquad\qquad [N5.6]$$

Note that P_s depends on the RNA-protein ratio since the average waiting time distribution, $p(t_w)$, depends on [TC] (see Eqs. [N5.1]-[N5.3]) while [TC] is proportional to R/P (Supp Note 3).

To relate P_s to the fraction of active ribosome equivalent, f_{active}, we assume that abortive translation does not occur for cells growing in rich medium. The fact that f_{active} does not reach 100% there (Fig. 3C, D of main text) is consistent with an earlier of the existence of a constant concentration of initiation-ready ribosomes, which clearly cannot participate in translation itself. Assuming that f_{active} is comprised of the remaining ribosomes that complete their translation, we have

$$f_{active} = 0.9 \cdot P_s \ . \qquad\qquad\qquad [N5.7]$$

The model defined by Eqs. [N5.1]-[N5.7] predicts a relation between the fraction of active ribosome equivalent, f_{active} and RNA-protein ratio, which is plotted as the red line in Fig. N3B. The active fraction is maximal and relatively constant at high RNA-protein ratio, and decreases sharply at a finite RNA-protein ratio due to abortive translation by stalled ribosomes. The

location of this drop is obtained by fitting the only adjustable parameter of the model, the abortive time $t_\times$, to the data (black circles). The drop predicted by this model is more abrupt than the data, possibly due to a number of neglected effects, e.g., a broad distribution of waiting times for different TC species, a broad distribution of protein length N, the effect of aborted translation of one ribosome on trailing ribosomes (Supplementary Fig. 12); moreover, the abortion time $t_\times$ itself may not be fixed and could be condition dependent. However, we see that such a simple model can already produce the essential features of a sharp drop in f_{active}. It serves here to illustrate a passive mechanism for the drop in active ribosomes under poor nutrients, which is an alternative to the active mechanisms suggested in Fig. 4A.
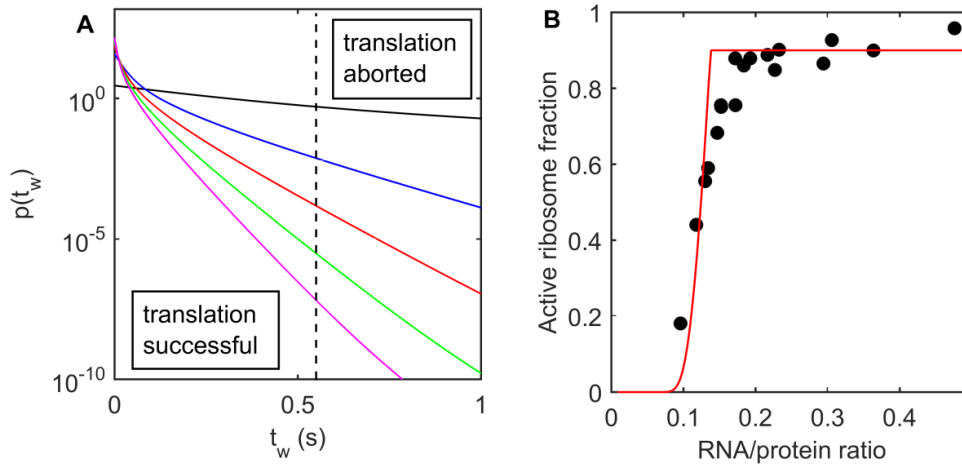
Fig. N3. Translation abortion can explain the decrease in active fraction at slow growth. (A) The probability distribution of times t_w that the ribosome spends waiting for the correct TC at each codon. The different colors show various levels of RNA/protein ratio (different concentrations of TC): 0.01 (black), 0.13 (blue), 0.26 (red), 0.38 (green), 0.5 (magenta). At lower RNA/protein ratio (poor nutrient), the distribution is much broader, indicating that the ribosome is waiting longer for each TC. The dashed line represents the cutoff time $t_\times$. We assume that translation is aborted for all $t_w > t_\times$, and the ribosome is considered inactive. (B) The active ribosome fraction deduced from the data (according to Supp Note 3) for nutrient limitation (black circles) and with the translation abortion model (red line). The fraction of active ribosome equivalent, f_{active}, was solved in the abortion model by substituting Eqs. [N5.1-N5.6] into Eq. [N5.7]. The parameters in the model were as much as possible obtained from experiment: k_{on} was determined from the fit to our data (Figure N1), and we used the measured tRNA abundances (a_c and b_c) from Supp Note 3B[17]. The f_{active} at high RNA/protein ratio was deduced from the data. The only free parameter is the translation abortion time $t_\times$, which we fit by requiring that the experimental data and the model agree at $f_{active} = 0.5$. The red line shows the correlation between the fractions of active ribosome equivalent, f_{active} and RNA/protein ratio as predicted by the model defined in Eqs. [N5.1]-[N5.7].

Supplementary Tables

Nutrient conditions	Growth rate (1/h)	Translational elongation rate (aa/s)
RDM + 0.2% glucose+10 mM NH_4Cl	1.8	16.7 ± 0.3
0. 2 % glucose+cAA+10 mM NH_4Cl	1.28	16.3 ± 0.1
10 mM glucose-6-phosphate+10 mM gluconate +10 mM NH_4Cl	1.12	16.1 ± 0.2
0.2% glucose+10 mM NH_4Cl	0.98	15.9 ± 0.2
0.2% xylose+10 mM NH_4Cl	0.75	14.9 ± 0.1
0.2 % glycerol+10 mM NH_4Cl	0.69	15.0 ± 0.2
0.2% fructose+10 mM NH_4Cl	0.69	14.7 ± 0.0
0.2% sorbitol+10 mM NH_4Cl	0.55	13.7 ± 0.2
0.2% galactose+10 mM NH_4Cl	0.5	13.1 ± 0.3
60 mM acetate+10 mM NH_4Cl	0.46	12.6 ± 0.2
0.2% mannose+10 mM NH_4Cl	0.41	13.0 ± 0.3
0.1% mannose+10 mM NH_4Cl	0.34	12.4 ± 0.1
NQ1261($\Delta ptsG$) strain in 0.2% glucose+10 mM NH_4Cl[a]	0.38	12.4 ± 0.2
20 mM potassium aspartate	0.33	12.0 ± 0.3
0.075% mannose+10 mM NH_4Cl	0.29	12.1 ± 0.1
0.2% glycerol +10 mM Arginine	0.20	11.6 ± 0.2
20 mM aspartate+10 mM NH_4Cl	0.23	12.3 ± 0.2
20 mM glutamate+10 mM NH_4Cl	0.13	10.7 ± 0.1
0.2% glycerol+20 mM Threonine	0.035	9.4 ± 0.3
Stationary phase	0	8.1 ± 0.2

Supplementary Table 1. *In vivo* **translational elongation rate of** *E. coli* **under nutrient limitation.** Wild type *E. coli* K-12 NCM3722 strain was grown in MOPS buffered minimal medium supplemented with various carbon and nitrogen sources. A broad range of growth rates were obtained. Typical variation between biological replicates (at least three times) for both the growth rate and translational elongation rate were within 5%. These data are shown in Fig. 1A.

[a] For this condition, we used a *ptsG* deletion strain (NQ1261) instead of the wild type strain. PtsG is the major transporter of glucose in *E. coli*. $\Delta ptsG$ strain can still utilize glucose as carbon source via the mannose PTS permease (ManXYZ), but with at a reduced efficiency[21]. Thus $\Delta ptsG$ strain grows in glucose medium with a much lower growth rate (0.38 h^{-1}) than wild type strain (0.98 h^{-1}). Hence, when growing in glucose medium, $\Delta ptsG$ strain can be treated as a type of carbon limitation similar to NCM3722 strain grown in a medium supplemented by a poor carbon.

		RDM+glucose (λ: 1.83 h^{-1})	Glucose (λ: 0.98 h^{-1})	Acetate (λ: 0.45 h^{-1})	Stationary phase (λ: 0 h^{-1})
AccA-LacZα (389 aa)	T_{first} (s)	32.6	32.5	39.2	58.2
	ER (aa/s)	17.2	17.3	13.3	8.07
CysK-LacZα (393 aa)	T_{first} (s)	33.8	34.7	41.2	56
	ER (aa/s)	16.5	15.9	12.6	8.55
FbaA-LacZα (429 aa)	T_{first} (s)	34.9	35	47	60
	ER (aa/s)	17.2	17.2	11.6	8.58
CarB-LacZα (1143 aa)	T_{first} (s)	73.9	75.7	93.4	139
	ER (aa/s)	17.9	17.4	13.7	8.86
LacZ (1024 aa)	T_{first} (s)	71.3	74.4	91.3	137.4
	ER (aa/s)	16.7	15.9	12.5	8.04
Average	**ER (aa/s)**	**17.1 ± 0.5**	**16.7 ± 0.8**	**12.7 ± 0.8**	**8.4 ± 0.4**

Supplementary Table 2 Translational elongation rate (ER) of several proteins under different nutrient conditions. The ER of several proteins other than LacZ were measured by translationally fusing each with the small LacZα fragment using a 10 aa linker (GGGGS)$_2$, so that the ER of each of these LacZα-fused proteins can be measured by the induction kinetics assay (similar with LacZ induction assay). The ER of LacZ for each corresponding growth condition is listed (last two rows) for comparison. The induction curve for each of the LacZα-fused protein after adding IPTG was obtained and the synthesis time of the first fused protein (T_{first}) was found using the Schleif plot (Supplementary Fig. 2 & Supplementary Fig. 7). ER was computed as $L/(T_{first}-10$ s), where L is the length of the fused protein containing target gene, linker and LacZα fragment included in the first column and 10 s is again taken to be the initiation time (Supplementary Fig. 3). ERs were characterized for four growth conditions covering the entire growth range from the fastest RDM+glucose condition to the stationary phase. The 4 proteins were chosen according to their lengths, with CarB being comparable to LacZ and the other three being around 300-400 aa (1/3 of the length of LacZ). Other criteria used in selecting these proteins are simple protein involved in metabolism, being free of unusual UTR flanking the coding gene. The row of "average" shows the average ER data of the five proteins as well as the standard deviation.

| Nutrient Conditions	Growth rate (1/h)	Total RNA (µg)/OD$_{600}$	Total Protein (µg)/OD$_{600}$	RNA/Protein
RDM+ 0.2% glucose+10 mM NH$_4$Cl	1.8	156 ± 4.2	327 ± 9.3	0.476
RDM+ 0.2% glycerol+10 mM NH$_4$Cl	1.57	138 ± 1.2	320 ± 6.5	0.431
0. 2 % glucose+cAA+10 mM NH$_4$Cl	1.28	115 ± 3	316 ± 10.5	0.364
0. 2 % lactose+cAA+10 mM NH$_4$Cl	1.17	106 ± 2.2	321 ± 4.1	0.33
10 mM glucose-6-phosphate +10 mM gluconate+10 mM NH$_4$Cl	1.12	99.1 ± 0.2	324 ± 1.5	0.306
0.2% glucose+10 mM NH$_4$Cl	0.98	97.9 ± 0.4	333 ± 4.4	0.294
0.2% lactose+10 mM NH$_4$Cl	0.99	88.7 ± 1.5	331 ± 8.7	0.268
0.2% arabinose+10 mM NH$_4$Cl	0.95	91.9 ± 3.2	338 ± 5.3	0.272
0.2% mannitol+10 mM NH$_4$Cl	0.92	87.3 ± 0.7	345 ± 2.3	0.253
0.2% xylose+10 mM NH$_4$Cl	0.75	84.8 ± 0.5	364 ± 14.1	0.233
40 mM sodium pyruvate+10 mM NH$_4$Cl	0.72	79.3 ± 3.2	367 ± 7.9	0.216
20 mM succinate+10 mM NH$_4$Cl	0.70	82.1 ± 0.9	365 ± 8	0.225
0.2 % glycerol+10 mM NH$_4$Cl	0.69	85.6 ± 1.4	377 ± 4.2	0.227
0.2% fructose+10 mM NH$_4$Cl	0.69	79.6 ± 0.2	367 ± 3.7	0.217
0.2% sorbitol+10 mM NH$_4$Cl	0.55	69.4 ± 2.3	360 ± 3.4	0.193
0.2% galactose+10 mM NH$_4$Cl	0.5	70.4 ± 1.6	383 ± 5.0	0.184
60 mM acetate+10 mM NH$_4$Cl	0.46	65 ± 2.9	378 ± 7.8	0.172
0.2% mannose+10 mM NH$_4$Cl	0.41	67.1 ± 1.6	390 ± 2.9	0.172
0.1% mannose+10 mM NH$_4$Cl	0.34	59.9 ± 3.9	394 ± 6	0.152
NQ1261(ΔptsG) in 0.2% glucose+10 mM NH$_4$Cl	0.38	63.8 ± 1.5	399 ± 9.2	0.160
20 mM potassium aspartate	0.33	59.1 ± 1.4	389 ± 2.6	0.152
0.075% mannose+10 mM NH$_4$Cl	0.29	58.4 ± 0.9	398 ± 0.9	0.147
0.2% glycerol +10 mM Arginine	0.20	40.43 ± 1.5	311 ± 5.6	0.130
20 mM aspartate+10 mM NH$_4$Cl	0.23	52.9 ± 0.4	395 ± 3.6	0.134
20 mM glutamate+10 mM NH$_4$Cl	0.13	46.1 ± 0.1	391 ± 7.7	0.118
0.2% glycerol+20 mM Threonine	0.035	27.8 ± 0.3	287 ± 3.1	0.097
Stationary phase	0	33.0 ± 0.4	384 ± 5.8	0.086

Supplementary Table 3 RNA-protein ratio (R/P) of *E. coli* under nutrient limitation. *E. coli* cells (NCM3722 unless otherwise indicated) was grown in MOPS buffered minimal medium supplemented with various carbon and nitrogen sources as indicated. The growth conditions are exactly the same as that shown in Supplementary Table 1. The R/P data are shown in Fig. 1D. Data of translational elongation rate in Supplementary Table 1 and R/P data of the same conditions in Supplementary Table 3 are plotted together and shown in Fig. 1E. Results of total RNA contents and total protein contents have been repeated for at least three times. The average values and errors displayed as ± standard error among replicates are listed in the table.

Nutrient conditions	Cm (μM)	Growth rate (1/h)	Translational elongation rate (aa/s)	Symbols
RDM+0.2% glucose +10 mM NH$_4$Cl	0	1.8	16.7 ± 0.3	◇ (green)
	4	1.08	16.8 ± 0.2	○ (green)
	8	0.57	17.3 ± 0.1	△ (green)
0.2% glucose +10 mM NH$_4$Cl	0	0.98	15.9 ± 0.2	◇ (red)
	2	0.71	16.0 ± 0.1	▽ (red)
	4	0.53	16.1 ± 0.2	○ (red)
	6	0.41	16.2 ± 0.2	□ (red)
	8	0.33	16.5 ± 0.1	△ (red)
	9	0.26	16.6 ± 0.4	⬡ (red)
0.2% fructose +10 mM NH$_4$Cl	0	0.69	14.7 ± 0.2	◇ (blue)
	4	0.35	15.9 ± 0.2	○ (blue)
	8	0.21	16.3 ± 0.1	△ (blue)
60 mM acetate +10 mM NH$_4$Cl	0	0.46	12.6 ± 0.1	◇ (orange)
	3	0.25	14.5 ± 0.3	○ (orange)
	6	0.18	15.6 ± 0.2	△ (orange)
20 mM potassium aspartate	0	0.33	12.0 ± 0.2	◇ (purple)
	2	0.24	15.3 ± 0.1	○ (purple)
	4	0.17	15.8 ± 0.2	△ (purple)
NQ1261(Δ*ptsG*) strain in 0.2% glucose+10 mM NH$_4$Cl	0	0.38	12.4 ± 0.2	◇ (tan)
	2	0.16	14.3 ± 0.1	○ (tan)
	3	0.092	15.2 ± 0.2	△ (tan)

Supplementary Table 4. *In vivo* **translational elongation rate of** *E. coli* **under chloramphenicol (Cm) inhibition.** Wild type *E. coli* NCM3722 cells were grown in medium with a fixed nutrient source and various amounts of Cm. In the last 3 rows, we also include a set of data for the Δ*ptsG* strain (NQ1261) grown in glucose medium to mimic poor carbon conditions. All the data are shown in Fig. 2A with corresponding symbols. Results of translational elongation rate have been repeated for at least three times. The average values and errors displayed as ± standard error among replicates are listed in the table.

Nutrient conditions	Cm (μM)	Growth rate (1/h)	Total RNA (μg)/OD$_{600}$	Total Protein (μg)/OD$_{600}$	RNA/Protein	Symbols
RDM+0.2% glucose +10 mM NH$_4$Cl	0	1.8	156 ± 4.2	327 ± 9.3	0.476	◇
	2	1.46	159 ± 2.1	321 ± 4.4	0.495	▽
	4	1.08	162 ± 5.6	294 ± 7.9	0.551	○
	6	0.87	163 ± 3.3	280 ± 4.6	0.582	□
	8	0.57	169 ± 2.9	272 ± 6.8	0.621	△
0.2% glucose + 10 mM NH$_4$Cl	0	0.98	97.9 ± 0.4	333 ± 4.4	0.294	◇
	2	0.71	113 ± 1.3	316 ± 7.7	0.358	▽
	4	0.53	128 ± 3.2	291 ± 0.4	0.440	○
	6	0.41	132 ± 2.2	271 ± 3.4	0.487	□
	8	0.33	138 ± 3.4	270 ± 4.8	0.511	△
	9	0.26	145 ± 1.6	255 ± 0.5	0.569	⬡
0.2% fructose + 10 mM NH$_4$Cl	0	0.69	79.6 ± 0.2	367 ± 3.7	0.217	◇
	2	0.46	99.5 ± 2.1	348 ± 7.4	0.286	▽
	4	0.35	107 ± 1.3	331 ± 8	0.323	○
	6	0.27	129 ± 3.2	319 ± 5.6	0.394	□
	8	0.21	138 ± 4.9	302 ± 9.3	0.457	△
60 mM acetate + 10 mM NH$_4$Cl	0	0.46	65 ± 2.9	378 ± 7.8	0.172	◇
	3	0.25	81.2 ± 3.8	330 ± 3.7	0.246	○
	6	0.18	93.7 ± 0.9	308 ± 5	0.304	△
20 mM potassium aspartate	0	0.33	59.1 ± 1.4	389 ± 2.6	0.152	◇
	2	0.24	86.8 ± 1	375 ± 6.6	0.231	○
	4	0.17	105 ± 2.8	360 ± 5.6	0.292	△
NQ1261(ΔptsG) in 0.2% glucose+10 mM NH$_4$Cl	0	0.38	63.8 ± 1.5	399 ± 9.2	0.160	◇
	2	0.16	75.2 ± 1.7	345 ± 8.7	0.218	○
	3	0.092	80.9 ± 2.2	321 ± 6.6	0.252	△

Supplementary Table 5 RNA-protein ratio (R/P) of *E. coli* under Cm inhibition. *E. coli* cells (NCM3722 unless otherwise indicated) were grown in medium with a fixed nutrient source and various amounts of Cm. The data of NQ1261 strain in glucose medium are also included. The growth conditions are exactly the same as that shown in Supplementary Table 4. The R/P data are shown in Fig. 2B with corresponding symbols. Data of translational elongation rate in Supplementary Table 4 and R/P in Supplementary Table 5 are plotted together as shown in Fig. 2C with the corresponding colored symbols. Results of total RNA contents and total protein contents have been repeated for at least three times. The average values and errors displayed as ± standard error among replicates are listed in the table.

| Nutrient source	Cm (μM)	Growth rate (1/h)	Fraction of active ribosome equivalent	Symbols
RDM + 0.2% glucose +10 mM NH$_4$Cl	0	1.8	0.958	◇
	4	1.08	0.505	○
	8	0.57	0.243	△
0.2% glucose +10 mM NH$_4$Cl	0	0.98	0.865	◇
	2	0.71	0.519	▽
	4	0.53	0.318	○
	6	0.41	0.222	□
	8	0.33	0.164	△
	9	0.26	0.123	⬠
0.2% fructose +10 mM NH$_4$Cl	0	0.69	0.888	◇
	4	0.35	0.290	○
	8	0.21	0.124	△
60 mM acetate +10 mM NH$_4$Cl	0	0.46	0.879	◇
	3	0.25	0.303	○
	6	0.18	0.170	△
20 mM potassium aspartate	0	0.33	0.756	◇
	2	0.24	0.282	○
	4	0.17	0.158	△
NQ1261(Δ*ptsG*) in 0.2% glucose +10 mM NH$_4$Cl	0	0.38	0.790	◇
	2	0.16	0.211	○
	3	0.092	0.099	△

Supplementary Table 6 Fraction of active ribosome equivalent (f_{active}) of *E. coli* under Cm inhibition. The growth conditions are exactly the conditions showed in Supplementary Table 4 and Supplementary Table 5. f_{acitve} is calculated according to the Supplementary Note 1 with the translational elongation rate data in Supplementary Table 4 and RNA/protein data in Supplementary Table 5. Data are shown Fig. 3A with corresponding symbols.

Growth conditions	Growth rate (1/h)	Fraction of active ribosome equivalent
RDM+ 0.2% glucose+10 mM NH$_4$Cl	1.8	0.958
0. 2 % glucose+cAA+10 mM NH$_4$Cl	1.28	0.9
10 mM glucose-6-phosphate +10 mM gluconate+10 mM NH$_4$Cl	1.12	0.927
0.2% glucose+10 mM NH$_4$Cl	0.98	0.865
0.2% xylose+10 mM NH$_4$Cl	0.75	0.902
0.2 % glycerol+10 mM NH$_4$Cl	0.69	0.849
0.2% fructose+10 mM NH$_4$Cl	0.69	0.888
0.2% sorbitol+10 mM NH$_4$Cl	0.55	0.879
0.2% galactose+10 mM NH$_4$Cl	0.5	0.860
60 mM acetate+10 mM NH$_4$Cl	0.46	0.879
0.2% mannose+10 mM NH$_4$Cl	0.41	0.756
NQ1261($\Delta ptsG$) in 0.2% glucose+10 mM NH$_4$Cl	0.38	0.790
0.1% mannose+10 mM NH$_4$Cl	0.34	0.751
20 mM potassium aspartate	0.33	0.756
0.075% mannose+10 mM NH$_4$Cl	0.29	0.683
20 mM aspartate+10 mM NH$_4$Cl	0.23	0.590
0.2% glycerol +10 mM Arginine	0.201	0.554
20 mM glutamate+10 mM NH$_4$Cl	0.13	0.441
0.2% glycerol+20 mM Threonine	0.035	0.168

Supplementary Table 7 Fraction of active ribosome equivalent (f_{active}) of *E. coli* under nutrient limitation. The growth conditions are exactly the conditions showed in Supplementary Table 1 and Supplementary Table 3. f_{active} is calculated according to the Eq. N1.5 of Supplementary Note 1 with the translational elongation rate data in Supplementary Table 1 and RNA/protein data in Supplementary Table 3. Data are shown as black circles in Fig. 3C.

Growth limitation	Growth conditions	Growth rate (1/h)	Total r-protein abundance ϕ_{Rb} (% proteome)
Nutrient limitation	0.2% glucose+10 mM NH$_4$Cl	0.98	11.6
	60 mM acetate+10 mM NH$_4$Cl	0.46	7.2
	0.075% mannose+10 mM NH$_4$Cl	0.29	5.1
	0.2% Glycerol+ 10 mM Arginine	0.20	6.1
	20 mM Glutamate+ 10 mM NH4Cl	0.12	4.7
	0.2% Glycerol+ 20 mM Threonine	0.03	4.4
Cm inhibition	Glucose 0 µM Cm	0.98	14.4
	Glucose 4 µM Cm	0.53	16.8
	Glucose 6 µM Cm	0.41	19.6
	Glucose 8 µM Cm	0.33	20.9

Supplementary Table 8 Total abundance of ribosomal proteins under nutrient limitation and Chloramphenicol inhibition. The absolute abundance of each ribosomal protein (r-protein) of *E. coli* NCM3722 cells (obtained by mass spectroscopy and tabulated in Supplementary Table 9) was added up to yield the total r-protein abundance for each growth condition. The results are expressed in "% of total cellular proteins" or "% proteome". In the text, the total r-protein abundance is taken to be the total ribosomal abundance (ϕ_{Rb}); see Supp. Note 1A.

Supplementary Table 9 Proteome abundances of individual r-proteins under nutrient limitation and Cm inhibition. Using quantitative mass spectroscopy (Supplementary Methods), we obtained the abundance of individual r-proteins relative to the reference condition (MOPS 0.2% glucose + 10 mM NH$_4$Cl) for *E. coli* NMC3722 cells grown in various conditions. The data for nutrient limitation was obtained in this work while the data for Cm inhibition was taken from Hui et al[14]. The relative abundance of each r-protein in each growth condition was then converted to absolute abundance (in % proteome) by using the absolute abundances of r-proteins of this strain grown in the reference condition, as provided in Supplementary Table 10.

Supplementary Table 10 Proteome abundance of individual r-proteins of the reference condition. The absolute abundances of individual proteins of NCM37222 cells grown in our reference condition (MOPS 0.2% glucose + 10 mM NH$_4$Cl) was estimated from the absolute abundances of proteins determined for a MG1655 strain using the ribo-seq method by Li et al[22]. To do so, we first used mass spectroscopy to obtain the relative abundance of proteins between NCM3722 cells grown in our reference condition and the MG1655 cells used by Li et al[22], grown in MOPS glucose condition used by Li et al[22] (see Supplementary Methods). Then the absolute abundances of each detected protein of NCM3722 cells was computed by multiplying the relative abundance of this protein between NCM3722 and MG1655 with the absolute abundance of the same protein in MG1655 as reported by Li et al[22]. For future reference, we list here not only the ribosomal proteins, but also all proteins detected in both NCM3722 and MG1655.

Nutrient conditions	Tet (µM)[a]	Growth rate (1/h)	Translational elongation rate (aa/s)	Symbols
0.2% glucose+10 mM NH4Cl	0	0.98	15.9 ± 0.2	
	1	0.76	16.2 ± 0.2	
	2	0.46	16.2 ± 0.3	◆
	3	0.32	16.1 ± 0.2	
	4	0.26	16.4 ± 0.1	
20 mM potassium aspartate	0	0.33	12.0 ± 0.2	
	2	0.24	14.6 ± 0.2	◆
	3	0.16	15.9 ± 0.1	
Nutrient conditions	Ery (µg/mL)[a]	Growth rate (1/h)	Translational elongation rate (aa/s)	Symbols
0.2% glucose+10 mM NH4Cl	0	0.98	15.9 ± 0.2	
	20	0.69	16.1 ± 0.1	
	60	0.54	16.4 ± 0.2	⬡
	120	0.33	16.5 ± 0.3	
20 mM potassium aspartate	0	0.33	12 ± 0.2	
	20	0.27	12.3 ± 0.1	
	40	0.18	13.9 ± 0.1	⬡
	60	0.11	16.0 ± 0.2	
Nutrient conditions	Mup (µg/mL)[a]	Growth rate (1/h)	Translational elongation rate (aa/s)	Symbols
0.2% glucose+10 mM NH4Cl	0	0.98	15.9 ± 0.2	
	12	0.73	14.0 ± 0.1	
	24	0.49	12.3 ± 0.2	◼
	60	0.28	11.7 ± 0.3	
Nutrient conditions	FA (µg/mL)[a, b]	Growth rate (1/h)	Translational elongation rate (aa/s)	Symbols
0.2% glucose+10 mM NH4Cl	0	0.96	16.0 ± 0.4	
	0.3	0.54	12.7 ± 0.1	
	0.6	0.32	9.0 ± 0.2	●
	1.2	0.26	8.3 ± 0.1	

Supplementary Table 11 *In vivo* **translational elongation rate of** *E. coli* **under the treatment of other antibiotics.** Cells were grown in MOPS minimal medium supplemented with various amounts of different types of antibiotics. All the data in this table are shown in Supplementary Fig. 13 with corresponding symbols. Results of translational elongation rate have been repeated

for at least three times. The average values and errors displayed as ± standard error among replicates are listed in the table.

[a] Abbreviations: Tet – Tetracycline; Mup – Mupirocin; Ery – Erythromycin. FA- Fusidic acid.
[b] This set of data was done for AS19 strain[23], a B/r derived strain which is permeable to fusidic acid. NCM3722 strain is not sensitive to fusidic acid due to its membrane impermeability to fusidic acid.

Nutrient conditions	Tet (μM)	Growth rate (1/h)	Total RNA (μg)/OD$_{600}$	Total Protein (μg)/OD$_{600}$	RNA/Protein	Symbols
0.2% glucose + 10 mM NH$_4$Cl	0	0.98	97.9 ± 0.4	333 ± 4.4	0.294	
	1	0.76	98.0 ± 4.7	312 ± 9.3	0.314	
	2	0.46	101 ± 3.4	316 ± 4.9	0.319	
	3	0.32	101 ± 2.8	308 ± 10	0.329	
	4	0.26	109 ± 1.9	297 ± 12	0.367	
	5	0.17	119 ± 1.1	283 ± 3.2	0.421	
20 mM potassium aspartate	0	0.33	63.6 ± 1.4	419 ± 2.6	0.152	
	2	0.24	98.9 ± 2.2	388 ± 11	0.255	
	3	0.16	110 ± 0.9	379 ± 8.2	0.291	

Nutrient conditions	Ery (μg/mL)	Growth rate (1/h)	Total RNA (μg)/OD$_{600}$	Total Protein (μg)/OD$_{600}$	RNA/Protein	Symbols
0.2% glucose + 10 mM NH$_4$Cl	0	0.98	97.9 ± 0.4	333 ± 4.4	0.294	
	20	0.69	110 ± 3.3	331 ± 8.0	0.333	
	60	0.54	114 ± 1.6	321 ± 13	0.356	
	120	0.31	135 ± 1	318 ± 7.0	0.424	
20 mM potassium aspartate	0	0.33	59.1 ± 1.4	389 ± 2.6	0.152	
	20	0.27	63.6 ± 0.6	388 ± 8.9	0.164	
	40	0.18	88.4 ± 3.3	378 ± 8.4	0.234	
	60	0.11	116 ± 2.3	375 ± 4.8	0.310	

Supplementary Table 12 RNA-protein ratio (R/P) of *E. coli* under Tetracycline (Tet) and Erythromycin (Ery) inhibition. Wild type *E. coli* NCM3722 cells were grown in two nutrient conditions supplemented with different amounts of Tet or Ery. The growth conditions are exactly the same as that shown in Supplementary Table 11. For conditions without drugs, the data are taken from Supplementary Table 3. The R/P data are shown at Supplementary Fig. 14A and B with corresponding symbols. Data of translational elongation rate of Tet and Ery in Supplementary Table 11 and R/P in Supplementary Table 12 are plotted together as shown at Supplementary Fig. 14C and D with the corresponding colored symbols. Results of total RNA contents and total protein contents have been repeated for at least three times. The average values and errors displayed as ± standard error among replicates are listed in the table.
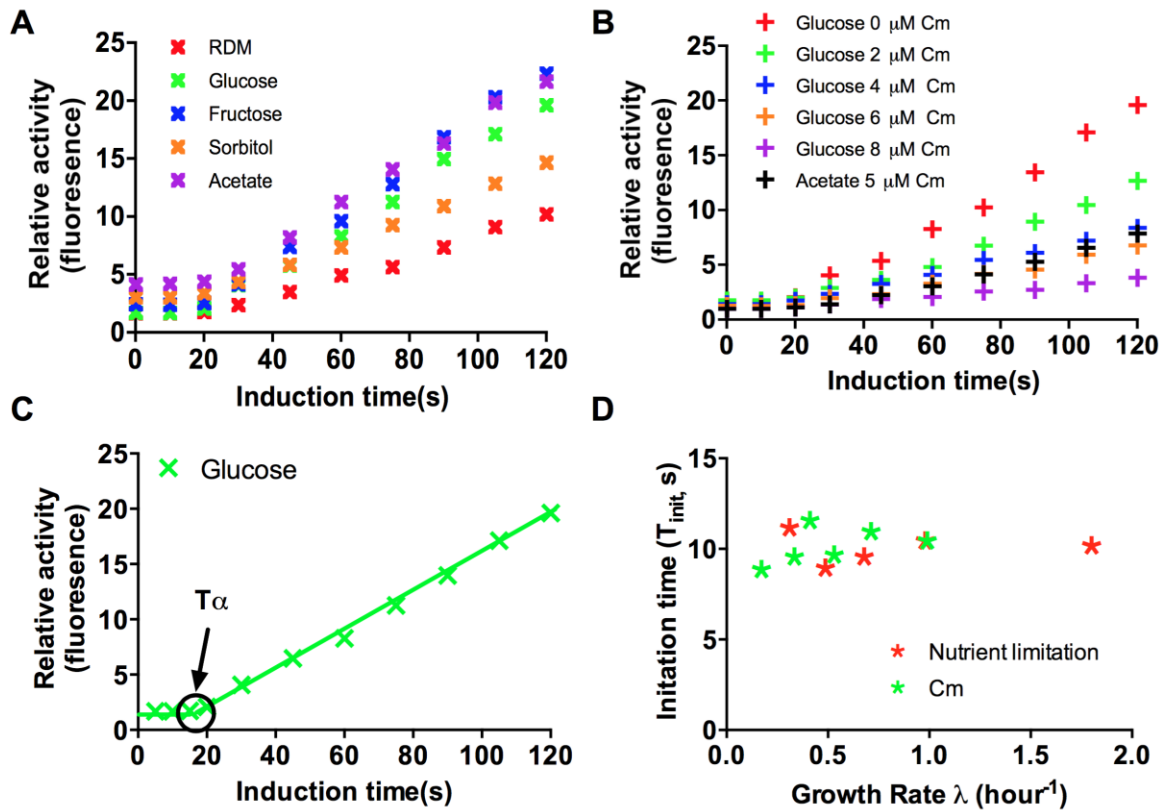
Supplementary Figures
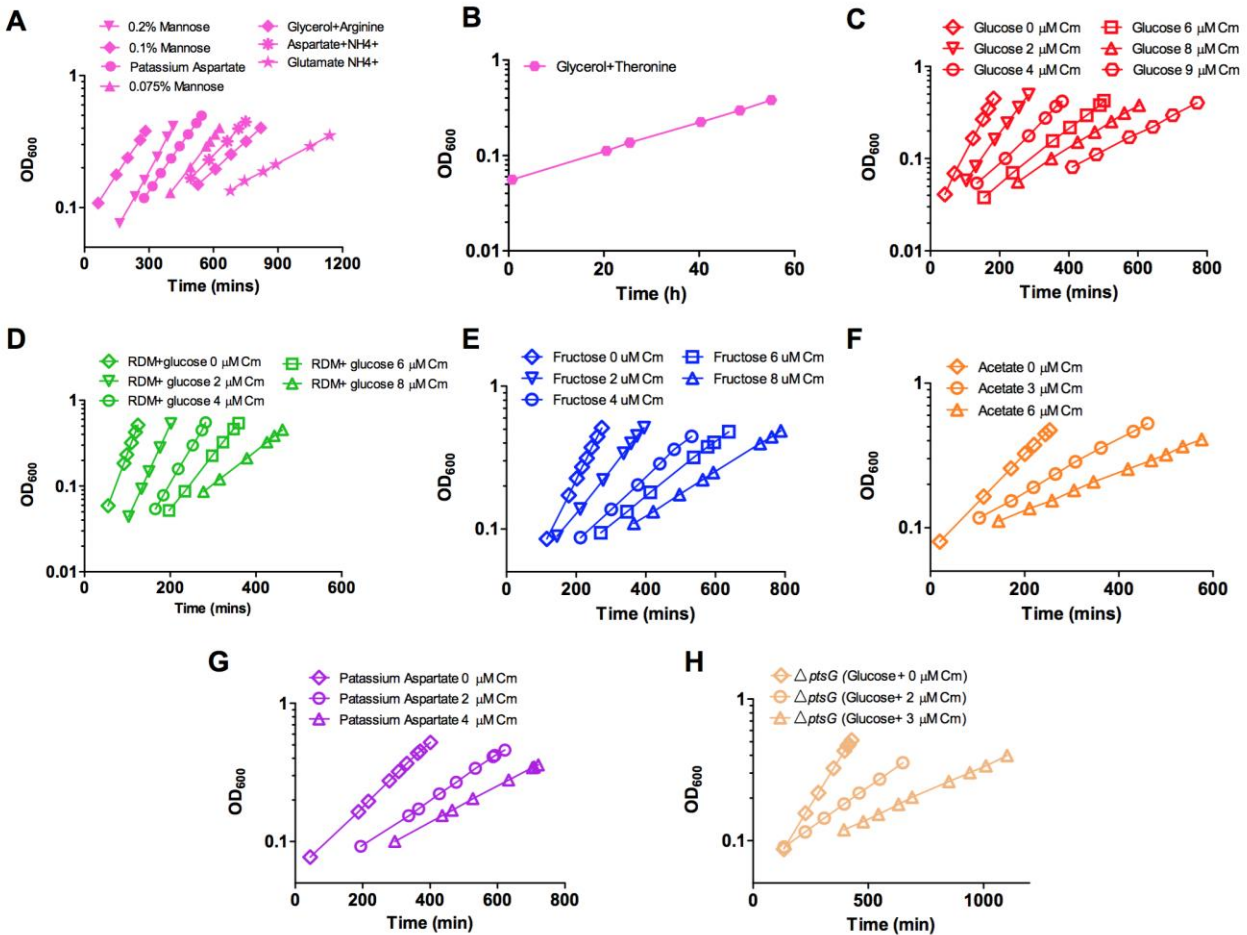
Supplementary Figure 1 Growth curves obtained for various growth conditions used in this study (A) Typical growth curves for cells growing in several poor nutrient conditions; (B) The growth curve for an extreme slow growth condition (Glycerol + Threonine, DT: 20 hours); (C) Growth curves for growth in glucose medium supplemented with different sublethal doses of chloramphenicol (Cm); (D) Growth curves in rich defined medium (RDM)+Glucose supplemented with different sublethal doses of Cm; (E) Growth curves in fructose medium supplemented with different sublethal doses of Cm; (F) Growth curves in acetate medium supplemented with different doses of Cm; (G) Growth curves in potassium aspartate medium supplemented with different sublethal doses of Cm; (H) Growth curves of ΔPtsG strain in glucose medium supplemented with different sublethal doses of Cm. Growth curves have been repeated for at least three times for all related conditions with one group of typical results shown above.
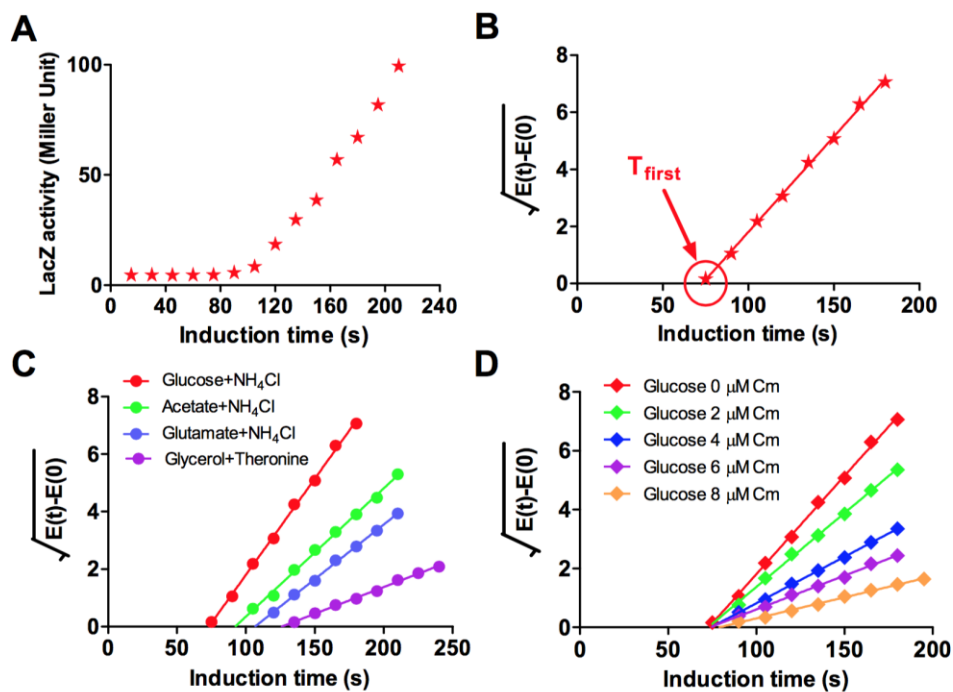
Supplementary Figure 2 Basic principle of translational elongation rate (ER) measured by *in vivo* β-galactosidase (LacZ) induction assay. Panels A and B show the raw data of the LacZ induction assay for cells grown in MOPS-buffered glucose medium. **A**. LacZ induction curve after addition of IPTG. LacZ activity of the culture was plotted against the induction time. **B**. The translation time of the first newly synthesized LacZ was obtained by using the Schleif plot[24]: The root square of the measured LacZ activity after adding IPTG ($\sqrt{E(t) - E(0)}$) was plotted against the induction time, where E(0) denotes the basal LacZ activity before it rises and is calculated by taking the average value of the first three points after adding IPTG, and E(t) is the enzyme activity at specific time points after adding IPTG. During the initial 2-3 mins, $\sqrt{E(t) - E(0)}$ exhibits a linear correlation with the induction time. The X-intercept of the line indicates the time for the ribosomes to finish translating the first full-length LacZ, and is denoted as T_{first}. In the classical LacZ induction assays[24], ER was obtained directly as the ratio of the length of LacZ (1024 aa) and the time T_{first}. We instead subtract the duration of the initiation steps as estimated in Supplementary Figure 3. The calculation of ER is detailed in Supplementary Method, in the section "Measurement of translation elongation rate". **C**. Several typical Schleif plots for cultures grown in various nutrient sources. Larger X-intercept indicates longer LacZ translation time, thus slower translational elongation rate. These plots show clearly that the translational elongation time increases for cells grown in poor nutrient conditions. **D**. Cm inhibition. The slope of Schleif plot reflects the rate of LacZ production. LacZ production rate is seen to decrease steadily for increasing dose of Cm inhibition. However, the similar X-intercept showed that the translational elongation time (hence rate) was hardly affected. The induction curve and corresponding Schleif plots have been repeated for at least three times (each one corresponds to one ER data) for all related conditions with one set of typical results shown above.

Supplementary Figure 3 Induction kinetics of the LacZα fragment. The induction time of the full length LacZ protein shown in Supplementary Figure 2 includes several initiation steps, including IPTG penetration into cells, LacI de-repression, RNA polymerase transcription initiation and ribosome translation initiation. In order to accurately compute the elongation time, we need to estimate and subtract away the initiation time. Towards this end, we performed a similar induction kinetics study for the LacZ alpha fragment (or LacZα, the N-terminal 1-90 aa fragment of LacZ)[25] for different growth conditions. Strain NQ1468 was used for measuring the induction kinetics of LacZα. For improved sensitivity, we used MUG assay instead of ONPG assay to quantify LacZ activity; see Methods. **A** LacZα induction kinetics obtained for cells grown in MOPS minimal medium with indicated substrate as the sole carbon source. **B** LacZα induction kinetics obtained for cells grown in varying sub-lethal doses of Cm with the indicated carbon source; **C** The estimate of the initiation time T_{init} from LacZα induction kinetics is illustrated using the example of cells grown in medium with glucose. First, the synthesis time of LacZα (T_α) was estimated by using flat line for the first few points and least-square line-fit for the remaining points. The x-coordinate of the intersection point, 16s is identified as T_α. We define the initiation time as $T_{init} = T_\alpha - 90/k$, where the 2nd term is the elongation time needed to complete the synthesis of the 90-residue long alpha fragment. As a first estimate of the elongation rate k, we used $k = 934aa/(T_{first} - T_\alpha)$, where T_{first} is the first appearance for the

full length LacZ as defined in Supplementary Fig. 2B. [T_{first} is found to be 74 s for glucose condition shown here.] $T_{\text{first}} - T_{\alpha}$ is the time to complete the translation of the remaining 934-residue of LacZ down stream of the alpha fragment. This yields $T_{\text{init}} \approx 10.4 \ s$ for the glucose condition. **D** T_{init} calculated for each growth condition studied, including nutrient limitation and Cm, is plotted against the growth rate. T_{init} is found to be always around 10 s for the conditions we examined. The induction curve shown in panel A and B have been repeated for three times for all related conditions with one group of typical results set shown above.

CH184 (SmP strain)

■ CH184 without str100
⊟ CH184 with str100

y-axis: $\sqrt{E(t)-E(0)}$

x-axis: Induction time(s)
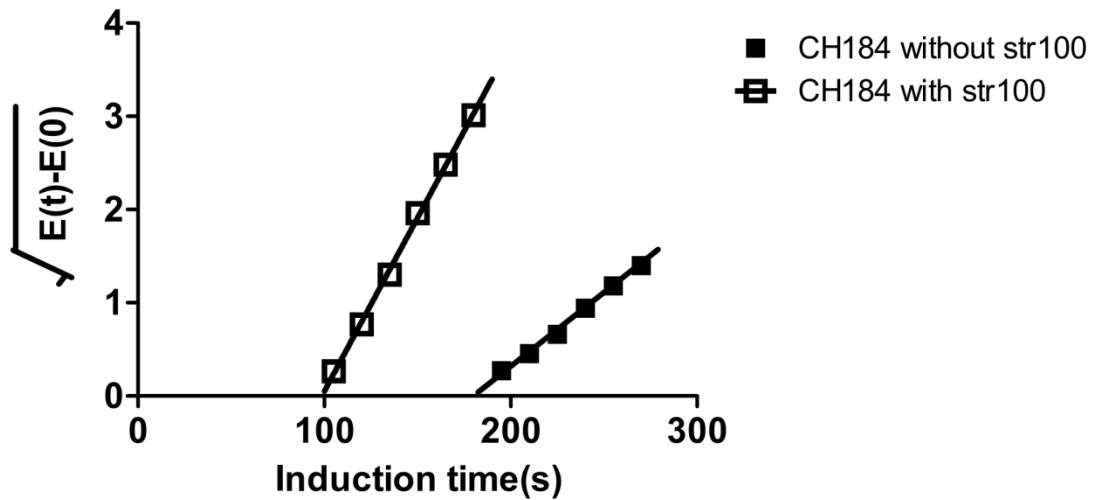
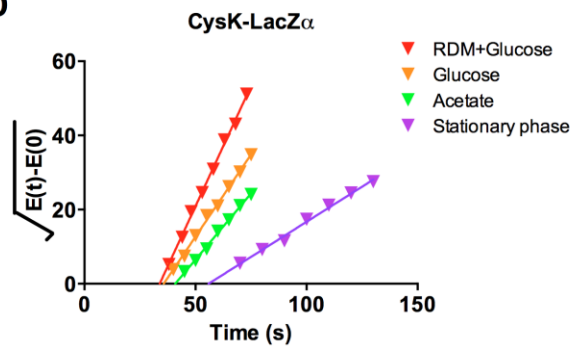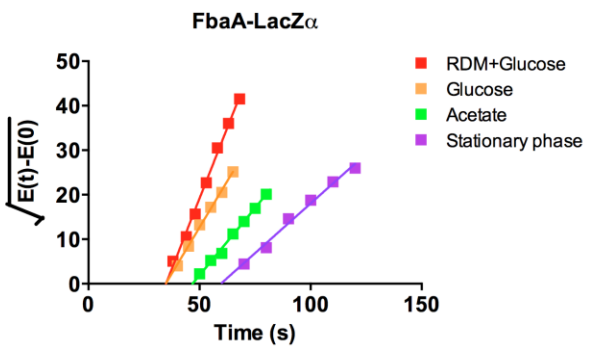| Data source	Translational elongation rate (aa/s)	
	No Streptomycin	100 μg/mL Streptomycin
This work	5.6 ± 0.4	11.3 ± 0.2
Ruusala et al[26]	5	11

Supplementary Figure 4 Translational elongation rate of CH184 strain. A typical example of translational elongation rate measured by LacZ induction assay is for CH184 strain. CH184 strain is a Streptomycin (Str) pseudo-dependent (SmP) strain[26,27]. SmP is a hyper-accurate ribosome mutant. The ribosome translates more accurately but much slower than wild type cells. Addition of 100 μg/mL streptomycin (Str100) reduces proofreading flow of the mutant ribosome and thus increases the translational elongation rate. CH184 grows in glucose plus casamino acids and nucleotides mixture with a doubling time (DT) of 98 mins. Str100 stimulates both the translational elongation rate as well as the growth rate (DT: 48 mins) by two-fold. The X-intercept of the Schleif plot for CH184 in the presence of streptomycin is approximately half of that for cultures without the drug, corresponding to a 2-fold translational elongation rate difference. The data have been repeated for three times with one typical Schleif plot shown above. The average values and errors displayed as ± standard error among replicates are listed in the table.
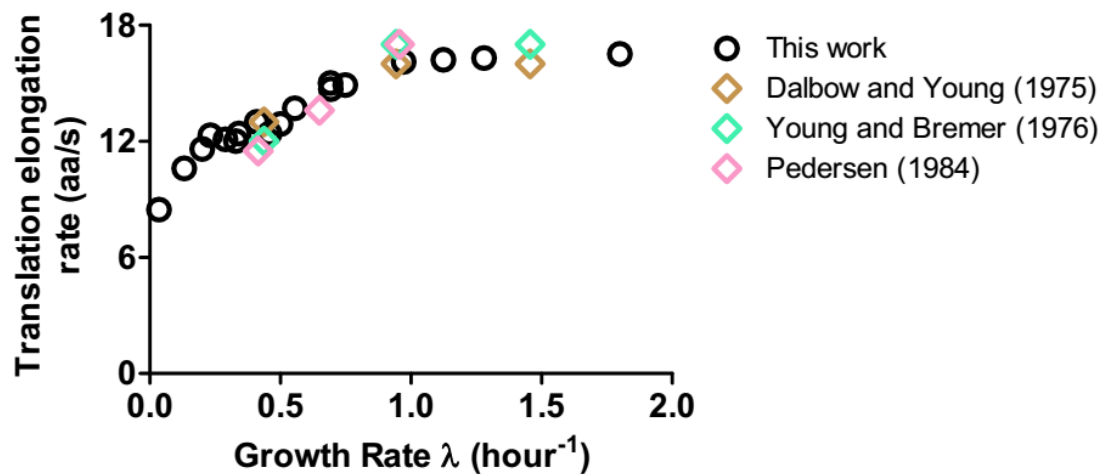
Supplementary Figure 5 Comparison of our data of translational elongation rate under nutrient limitation with earlier reports. Data points are obtained from Dalbow et al, Young et al, and Pedersen et al[28-30]. In the past several decades, generally there were two major ways for measuring translational elongation rate, one is LacZ induction assay, the other is pulse-chase radioactive labeling. To our knowledge, translational elongation rates obtained from these two methods were always consistent with each other. In the above plot, translational elongation rate data of Young et al (cyan squares), and Pedersen et al (pink squares) were measured by pulse-chase radioactive labeling. This method can in principle measure the translational elongation rate of various proteins, not only related to LacZ. Dalbow et al (brown squares) measured translational elongation rate also by LacZ induction assay. The results of all three data sets are similar with the results in this work. The conclusion is that, translational elongation rate keeps nearly constant at fast growth, but decreases in slow growth. The consistence between the two methods clarifies that the translational elongation rate obtained for LacZ can also largely represent the results for other proteins.
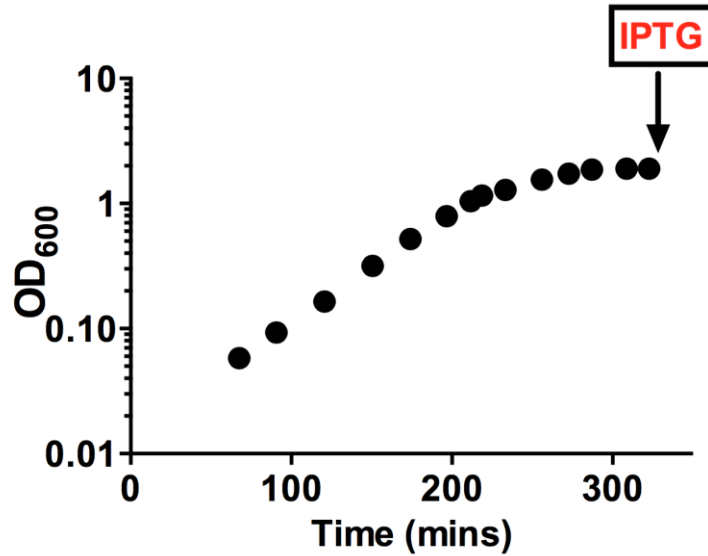
Supplementary Figure 6 *E. coli* cells grown to the stationary phase. Wild type *E. coli* NCM3722 strain was grown in Glucose+cAA medium to stationary phase, with the culture saturating at $OD_{600} \approx 1.9$. IPTG was added at approximately 1 hour after OD stopped increasing to induce the *lac* operon for measuring translational elongation rate using LacZ induction assay as shown in Fig. 1B. Growth curve has been repeated for at least three times with one typical result shown here.
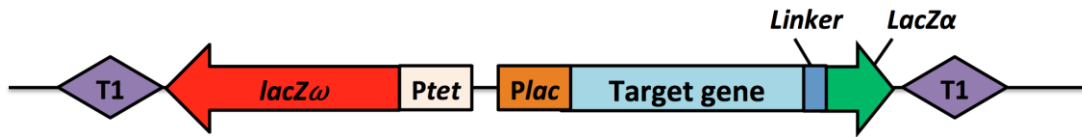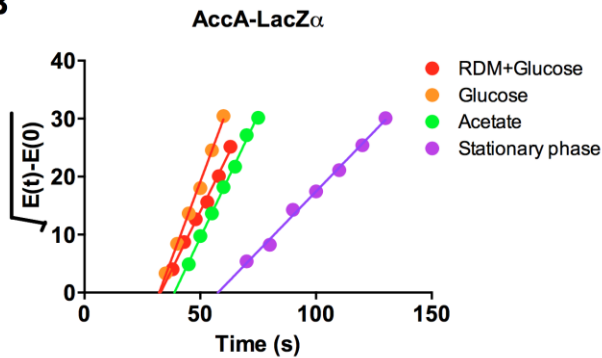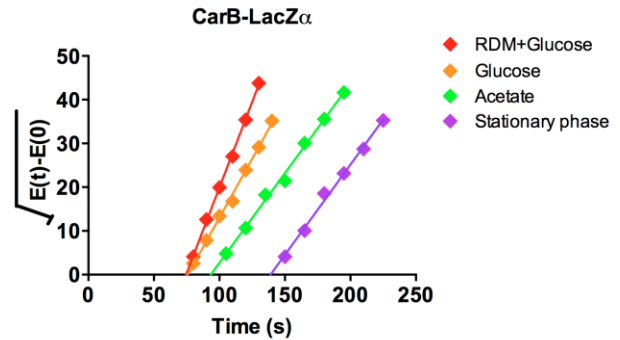
Supplementary Figure 7 Translational elongation rate (ER) of several other proteins under different nutrient conditions. (A) Translational elongation of several proteins other than LacZ was studied by translationally fusing each of them with the small LacZα fragment using a short peptide linker $(GGGGS)_2$ and placing the fused protein under the control of native *Plac* promoter. The complementary LacZω fragment is expressed by a constitutive *Ptet* promoter; see Methods. The construct is placed in a low copy pZS24*-MCS plasmid. As a result, the ER of all the LacZα fused proteins can be measured by the induction kinetics assay, which is similar to LacZ induction assay and described in Method and the caption of Supplementary Fig. 2. These proteins are selected based on their lengths, with CarB being comparable to LacZ and the other three being around 300-400 aa (1/3 of the length of LacZ). Other criteria used in selecting these proteins are simple protein involved in metabolism, being free of unusual UTR flanking the coding gene. **B)** Schleif plot of AccA- LacZα protein; **(C)** Schleif plot of CarB-LacZα protein. **(D)** Schleif plot of CysK-LacZα protein. (E) Schleif plot of the FbaA-LacZα. Schleif plot from panel B to E has been repeated for at least three times with one typical result shown here.
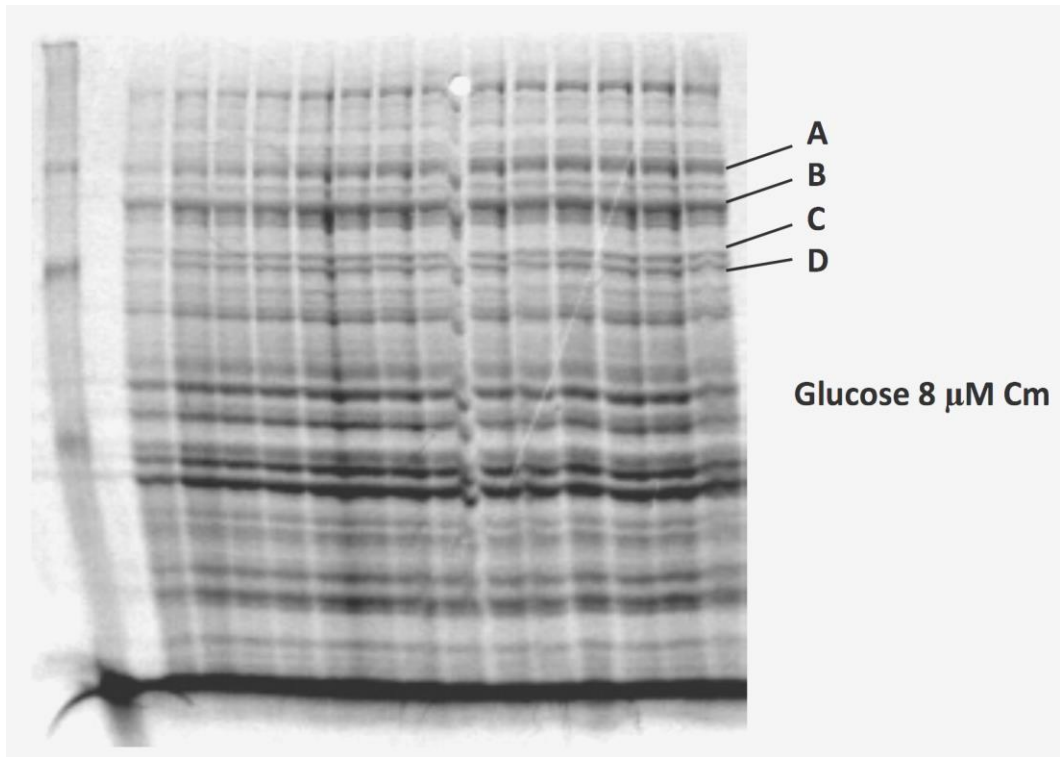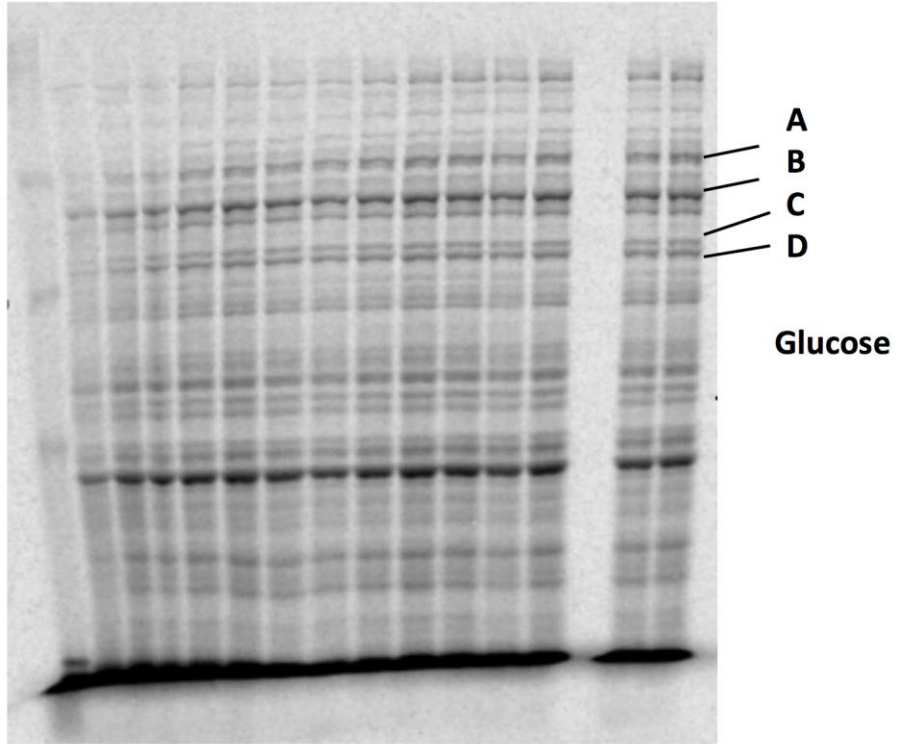
38
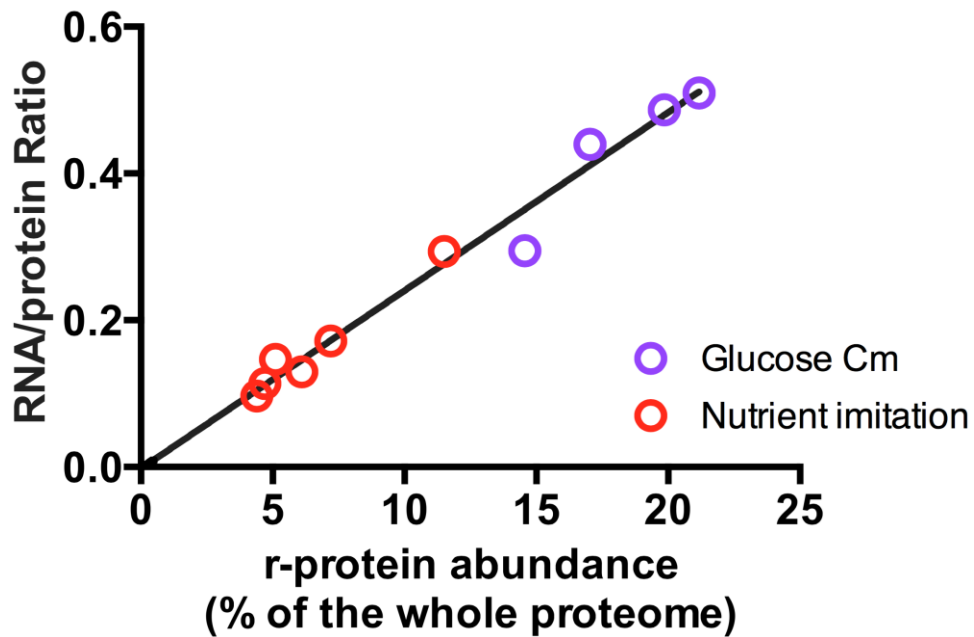
Supplementary Figure 8 Correlation between Ribosome protein (r-protein) abundance with RNA/protein ratio upon both nutrient limitation and Cm inhibition. Protein abundance data are from Supplementary Table 8-10. The data on RNA/protein ratio are obtained from Supplementary Table 3 and Table 5. A linear correlation is obtained with the linear regression coefficient $R^2 = 0.98$ and with a slope of 2.4. The r-protein abundance data are the average value of more than 3 individual peptides for each r-protein.
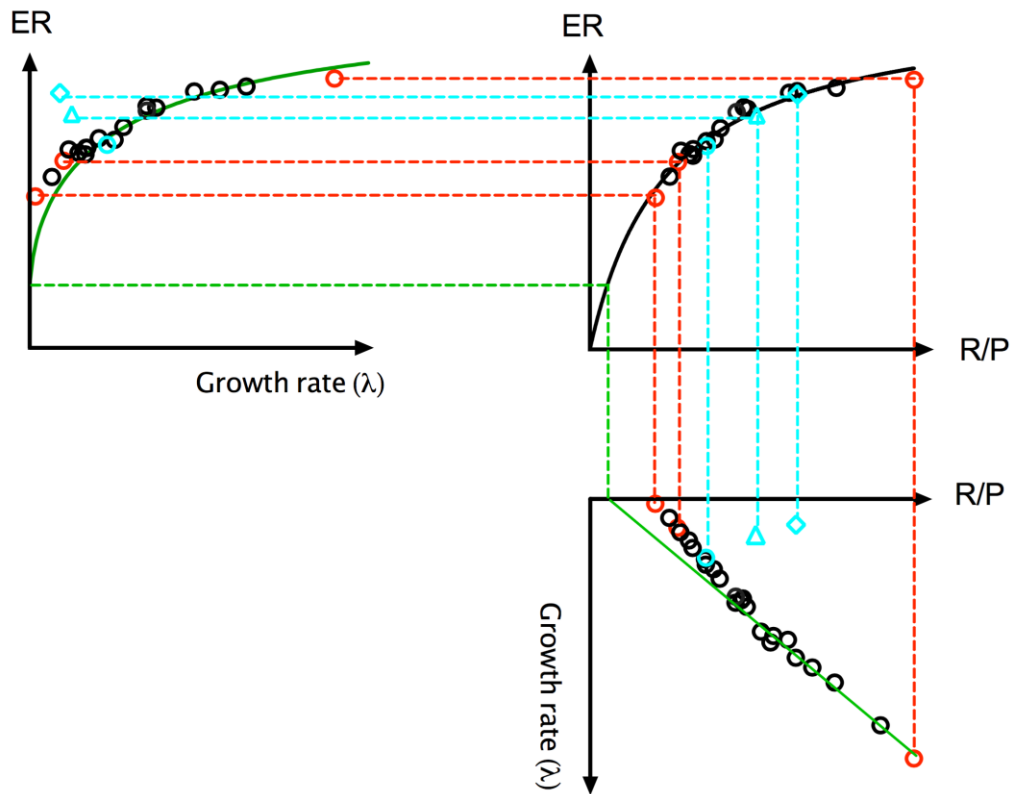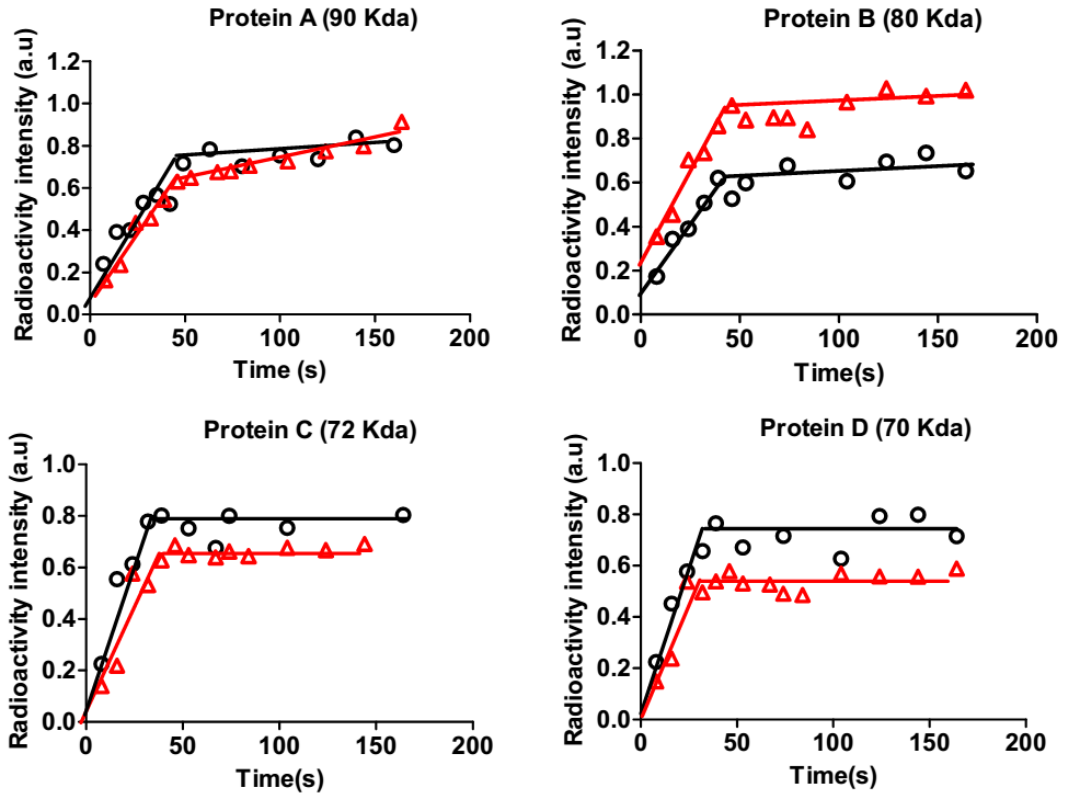
Supplementary Figure 9 A tight coupling between ribosome content and the translational elongation rate. The Michaelis-Menten relation between the elongation rate (ER) and the ribosome content as quantified by the RNA/protein ratio (R/P), shown as the black curve above and supported by the data of Fig. 1E and 2C, enforces a link between the growth rate dependence of ER (Fig. 1A, 2A) with the growth rate dependence of the ribosome content (Fig. 1D, 2B) as illustrated by the colored dashed lines here: The red (and black) symbols indicate the results for nutrient limitation. Note that if R/P follows a simple linear relation with the growth rate throughout (as indicated by the solid green line), then the ER at zero growth would be much smaller as indicated by the position of the dashed green line. The same plot illustrates that under increasing doses of Cm inhibition, the rise of R/P at reduced growth rate (cyan symbols) leads to the counter-intuitive rise of ER at slow growth.

A

A
B
C
D

Glucose

A
B
C
D

Glucose 8 μM Cm

B

Protein A (90 Kda)

Protein B (80 Kda)

Protein C (72 Kda)

Protein D (70 Kda)

Conditions	GR (1/h)	Symbol	Translation elongation rate (aa/s)				
			Protein A (800 aa)	Protein B (710 aa)	Protein C (640 aa)	Protein D (620 aa)	LacZ (1024 aa)
Glucose	0.98	○	17.3	16.6	16.5	16.9	15.9
Glucose 8 µM Cm	0.35	△	17.3	16.4	16.8	17.2	16.5

Supplementary Figure 10 Translational elongation rate obtained by pulse-chase radioactive methionine labeling. The translational elongation rates obtained for cells grown under chloramphenicol (Cm) treatment (Fig. 2A) are different from the common expectation. To rule out the possibility that these results are specific to LacZ protein, we supplemented the LacZ induction assay with a second approach, using pulse-chase radioactive methionine labeling to measure the elongation rate of different proteins[28]. The basic principle of this method is as follows: For exponentially growing cells, we add [S35] labeled methionine so it will enter into cytoplasm and be incorporated in polypeptide synthesis. After 10 s (we take this as time "zero"), we quickly add excess amount of unlabeled methionine to immediately inhibit the further incorporation of [S35] methionine. During this 10-second pulse, all nascent chains are labeled by [S35] (because there are Met codons throughout the gene). So the first full-length products observed would have their C-termini radiolabeled, subsequent products would have their mid-regions labeled, and the last products observed would have their N-termini labeled. When the synthesis of the protein products with their N-termini labeled has also been finished. The

band in a SDS-PAGE gel of a specific protein will reach saturation and the corresponding time point (corresponding to the location of change in slope shown in the plots) indicates the time needed for the translational elongation of this entire protein.

In the SDS-PAGE gel, we obtained four protein bands that were well resolved (Panel A). The molecular weights (MW) of the proteins were known from the protein size markers. The lengths of the four analyzed proteins were then obtained through dividing protein MW by 110 (average MW of amino acids). With the synthesis time of the four proteins (the turning point of the plot when the bands intensity reaches saturation) obtained from the plot in Panel B, we obtained the translational elongation rates for all of them as shown in the Table below the plots. Our data shows that adding Cm doesn't affect the translational elongation rate in glucose medium, in agreement with the results obtained from LacZ induction assay. The data have been repeated for three times with one typical result shown here.
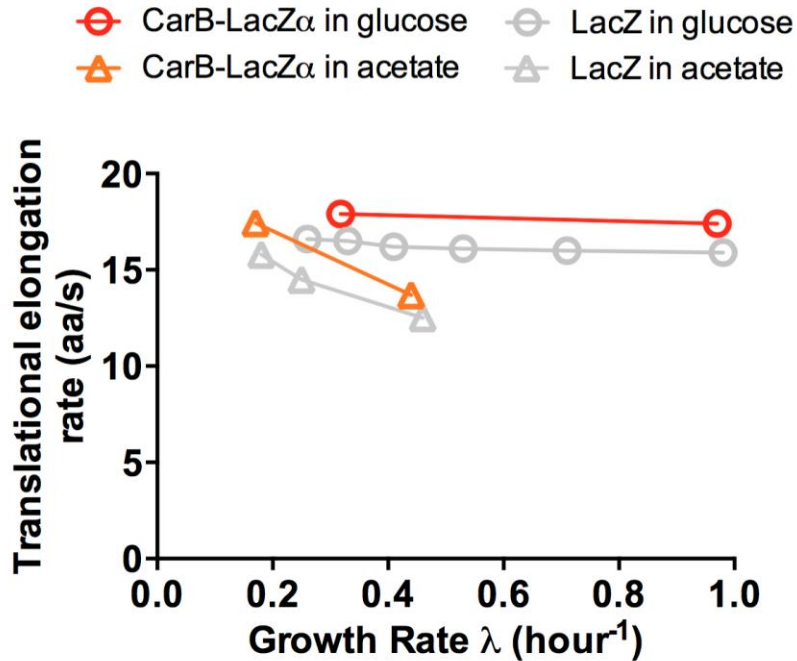
| Growth condition	Growth rate (1/h)	Translation elongation rate (aa/s)	
		CarB-LacZα	LacZ
Glucose 0 μM Cm	0.98	17.4	15.9
Glucose 8 μM Cm	0.33	17.8	16.5
Acetate 0 μM Cm	0.45	13.7	12.5
Acetate 8 μM Cm	0.17	17.3	15.8

Supplementary Figure 11 Translational elongation rate (ER) of CarB-LacZα protein upon Cm addition. In addition to the pulse-chase labeling data in Supplementary Figure 10, we further measure the ER of CarB-LacZα protein upon Cm addition in both glucose medium and acetate medium. The results obtained (red and orange) are in general agreement with the data from full-length LacZ (gray). Together with the pulse-chase labeling data in Supplementary Figure 10, this shows that the ER obtained using LacZ (Figs 1 and 2) is not specific to LacZ protein. Data points here are the average values of three replicates.
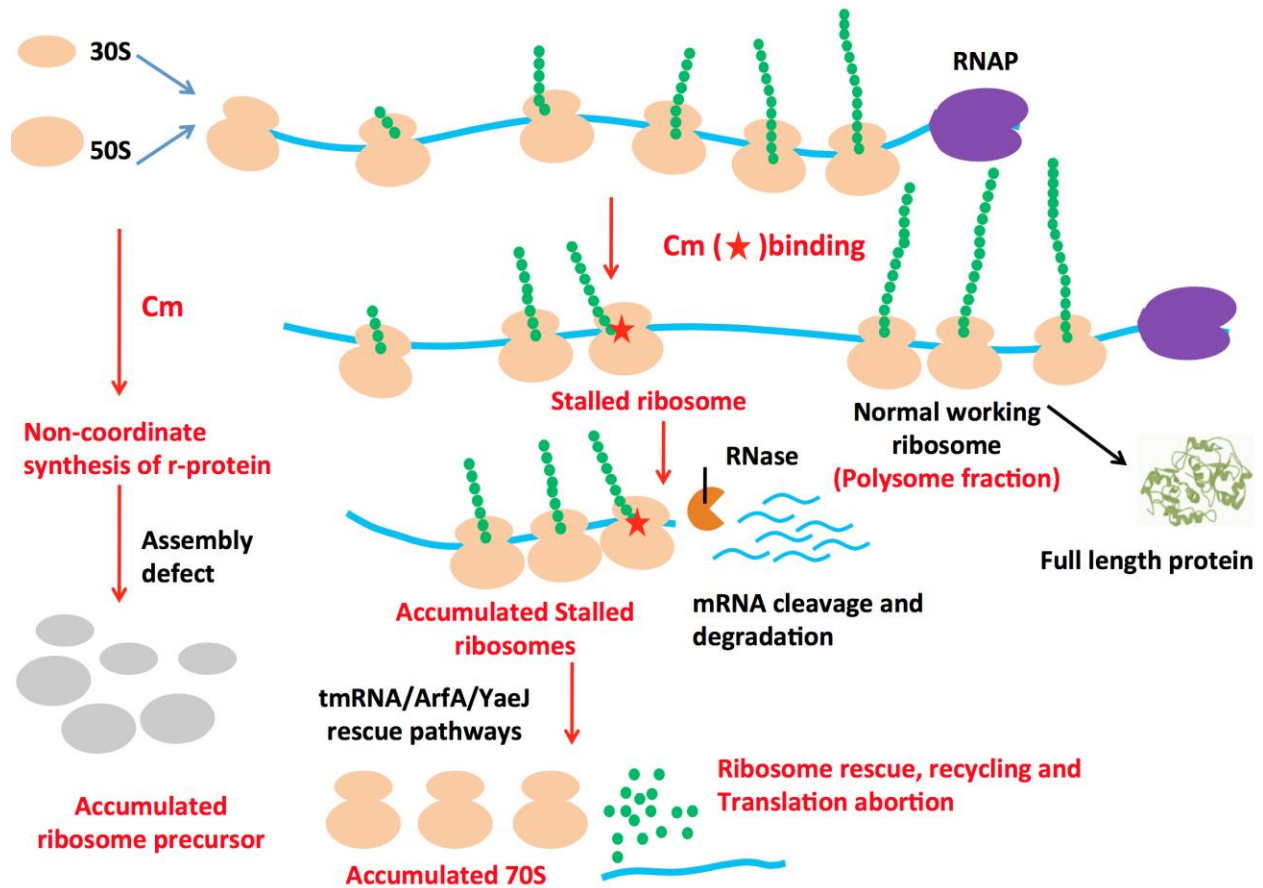
Supplementary Figure 12 An *in vivo* model of protein synthesis inhibition by chloramphenicol. For cells in normal growth conditions, translating ribosomes exist in the forms of polysomes, where several ribosomes bind to the same mRNA, following RNA polymerase (RNAP, purple) for polypeptide synthesis. Under Cm treatment, once a translating ribosome contained in polysome is hit by a Cm molecule and binds tightly to it (the off-time is ~12 mins on average)[9], it would stall along the mRNA as indicated by the red star in the illustration. [Calculation in Supp. Note 2 shows that the probability of continuing to translate after being hit is < 1%.] The trailing ribosomes would be stalled as well[31] while RNAP and the unaffected ribosome(s) would continue to move forward. This leaves an mRNA gap between the translating and stalled ribosomes, thereby allowing mRNA degradation by RNase[10]. The unaffected leading ribosome(s) would go on to complete protein synthesis, yielding a translational elongation rate indistinguishable from untreated cells. The stalled ribosomes would get rescued by some ribosome rescue pathways (e.g., tmRNA-SmpB/ArfA/YaeJ)[20,32-34], leading to an increased amount of 70S ribosomes. The partially synthesized nascent peptides will likely be further degraded[35,36], making the ribosomes synthesizing them effectively "inactive" in the sense that they don't produce stable protein products.

Biochemical evidences exist in the literature supporting various pieces of the above model:

a) Uemura et al[11] directly observed ribosome arrest in vitro by erythromycin, which exerts a similar effect on ER as Cm in vivo (Supplementary Figure 13B, 14B and 14D). On the other hand, fusidic acid (which has a fast off-rate) mainly decreased the overall elongation rate, again consistent with our *in vivo* ER data.

b) Pato et al[37] directly observed the decoupling between RNA polymerase and the trailing ribosomes upon Cm treatment: The promoter distal (3') portion of mRNA (the gap between ribosome and RNAP), synthesized after ribosomes had been immobilized by Cm on the promoter proximal (5') portion of the mRNA, was subsequently degraded due to the lack of protection by translating ribosomes.

c) Harvey et al [9] found (as we did in Supplementary Figure 20) a strong increased in 70S monosome fraction under Cm treatment. They showed that this 70S fraction contributed little to the overall protein synthesis compared to the smaller polysome fraction, demonstrating that 70S monosome fraction are mostly inactive fraction. At the same time, the few leading ribosomes that have managed to escape from binding to Cm can work normally and be seen as polysomes that contribute to most of the protein synthesis.

d) There is also the known effect of Cm interfering with the ribosome assembly process[38], demonstrated by the substantial increase in ribosome precursor fraction (between 20S and 50S in the polysome profile of Supplementary Fig. 20) which was also reported by Harvey et al[9])[993636]. Similar behaviors have also been observed for chlortetracycline and erythromycin[38,39].
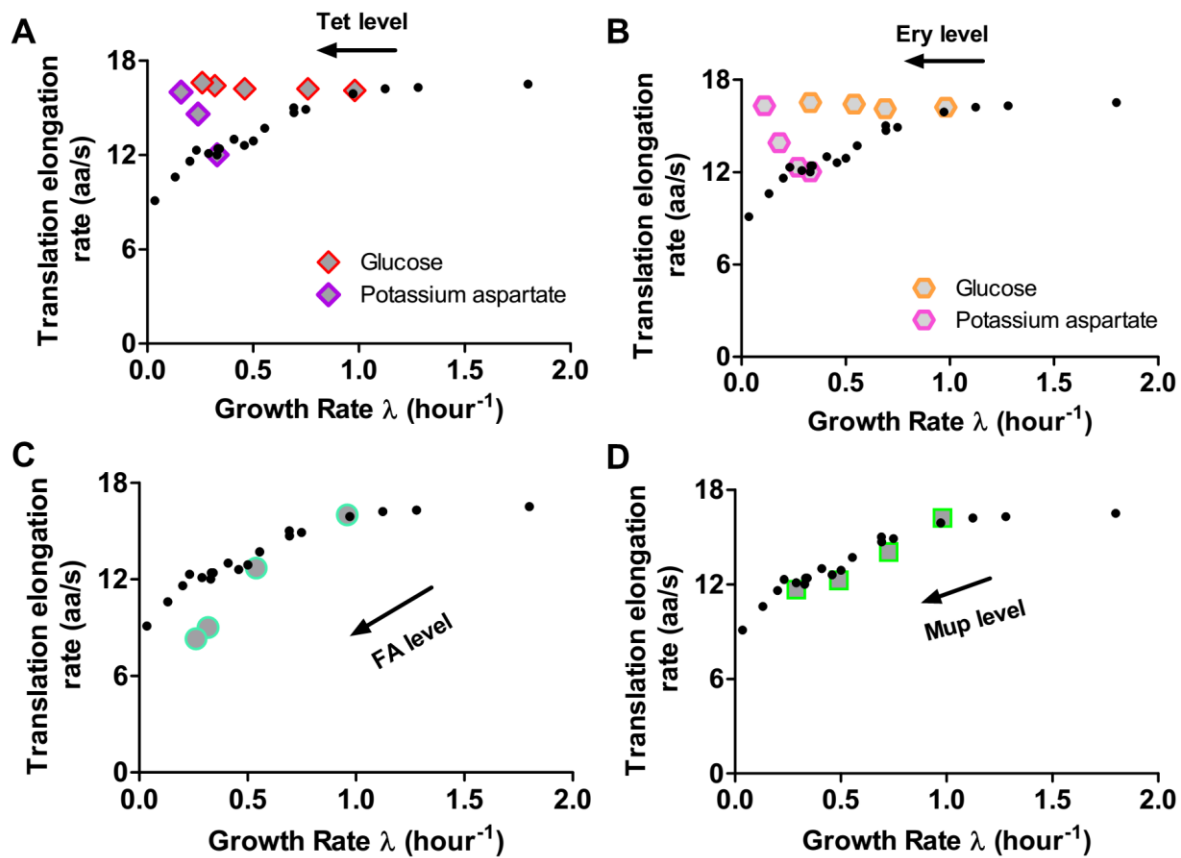
Supplementary Figure 13 Translational elongation rate under sublethal doses of other drugs.
A. Tetracycline (Tet). **B.** Erythromycin (Ery). **C**. Fusidic acid (FA). **D.** Mupirocin (Mup). The original data (the average value of at least three replicates) in this figure are given in Supplementary Table 11. The small black dots in all the panels represent the translational elongation rate upon nutrient limitation as shown in Fig. 1A.
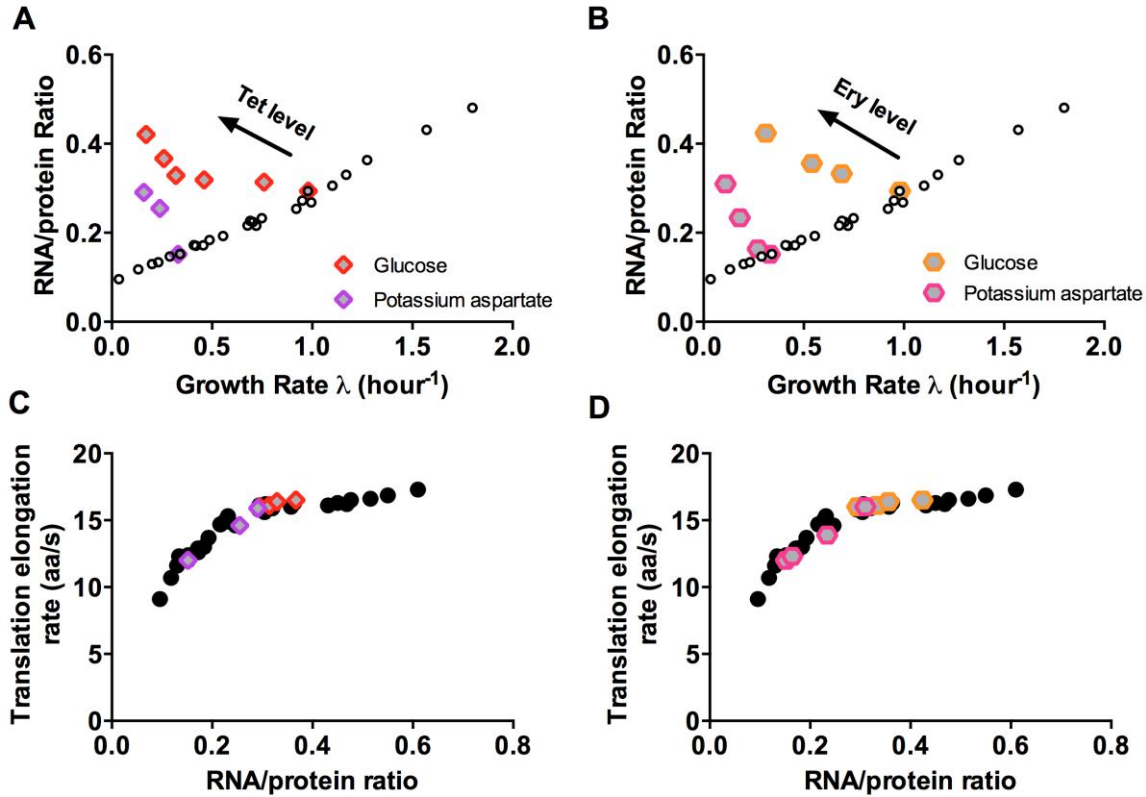
Supplementary Figure 14 Translational elongation rate versus RNA-protein ratio under Tetracycline (Tet) and Erythromycin (Ery) inhibition. A RNA-protein ratio (R/P) upon sub-lethal doses of Tet at two nutrient conditions: Glucose (good nutrient), potassium aspartate (poor nutrient). Original data are given in Supplementary Table 12. The black open circles indicate the R/P under nutrient limitation as shown in Fig. 1D. Similar to Cm, Tet inhibits protein synthesis by interfering with the translational elongation process[40]: it binds to the 30S subunit of ribosome, blocking the attachment of charged tRNA to the A site on the ribosome[40]. Also similar to Cm, Tet suppresses the internal level of ppGpp, causing up-regulation of ribosomal synthesis[41]. **B** Same as panel A, but for Ery rather than Tet. Ery binds to the 50S subunit of ribosome, blocking the peptide exit tunnel of ribosome (Recent study has instead shown that its main mode is context-specific inhibition of peptide bond formation)[42,43]. Its effect on ppGpp and ribosomal synthesis is also similar to Tet and Cm[44,45]. **C** Translational elongation rate versus R/P for Tet. Original data of translational elongation rate and R/P upon Tet listed at Supplementary Table 11 and Table 12 are plotted against each other. The black circles represent the data of nutrient limitation and Cm inhibition shown in Fig. 2C. We can see clearly that the colored and black datasets overlap with each other. **D** Translational elongation rate versus R/P ratio for Ery. Original data of translational elongation rate and R/P ratio upon Ery listed at Supplementary Table 11 and Table 12 are plotted against each other. The black symbols are the same as in panel C. Like Tet, the colored and black datasets overlap with each other. Data points in panel A and panel B are obtained from the average value of at least three replicates for total RNA content and total protein content listed in Supplementary Table 12.
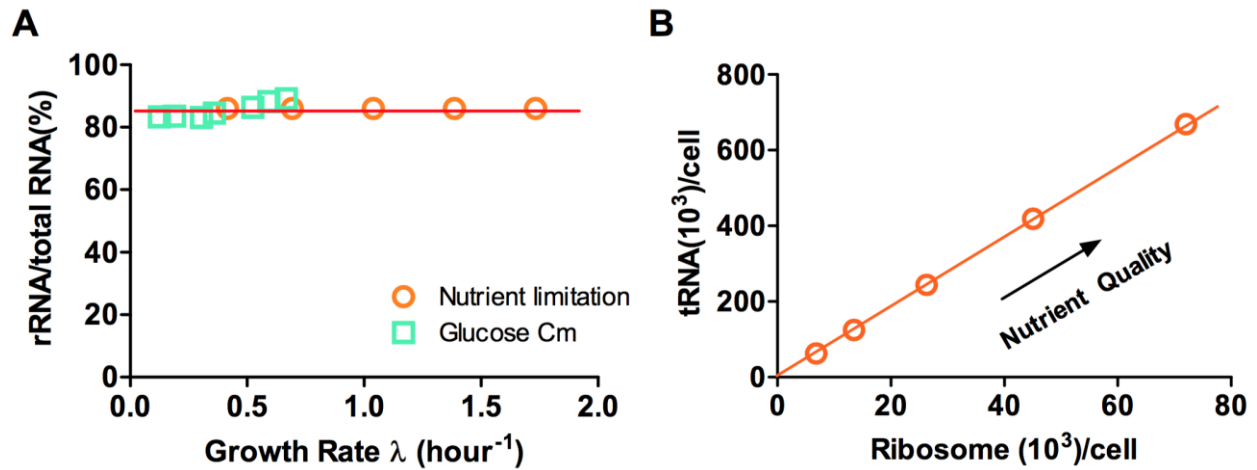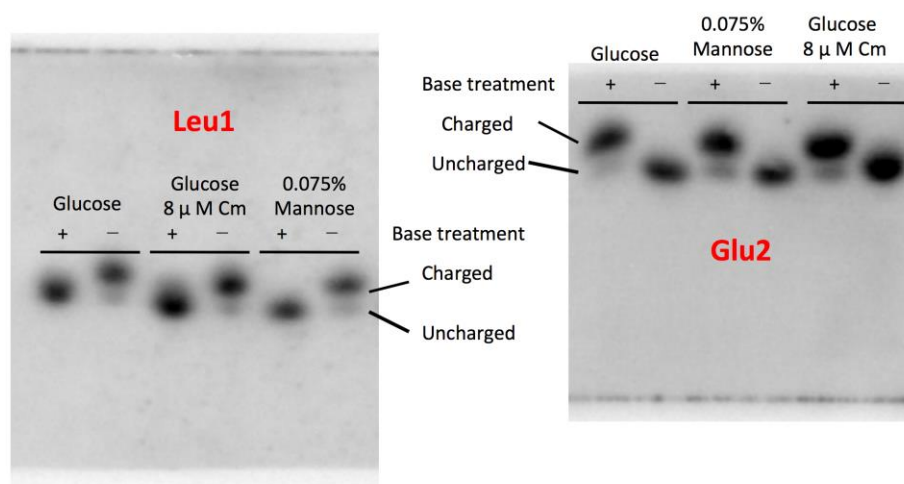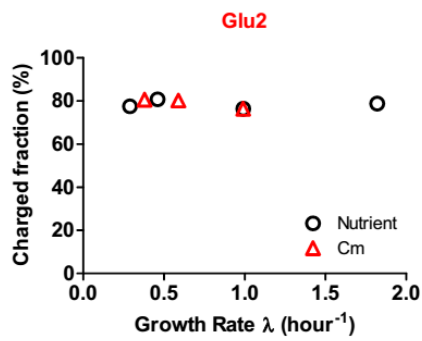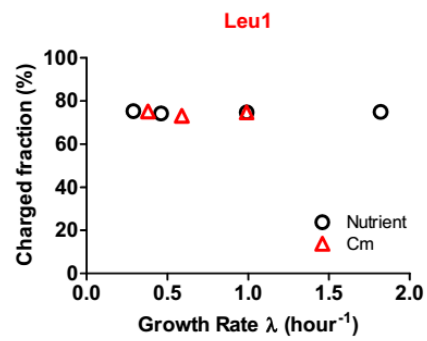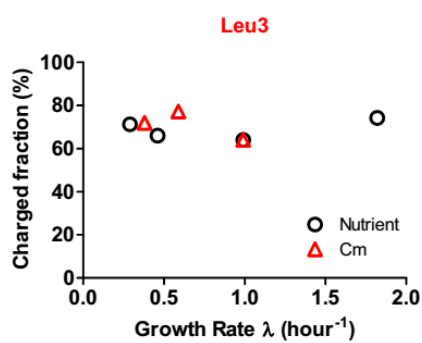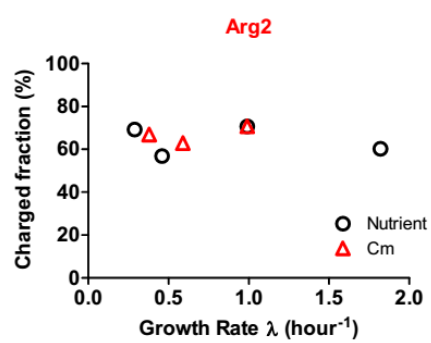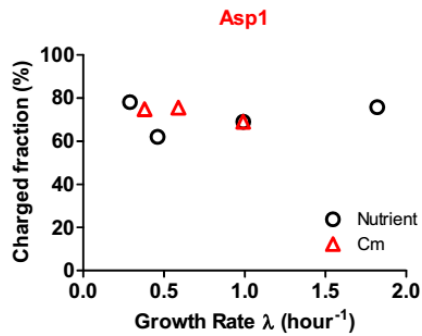
Supplementary Figure 15 rRNA and tRNA abundances. (A) The ratio of rRNA to total RNA in both nutrient limitation[5] and chloramphenicol treatment[9] are plotted against the growth rate. This ratio is seen to remain constant at ~86%. As the remaining RNA is mostly tRNA, the data suggest tRNA/rRNA ratio is also constant. This is expected as rRNA and tRNA are co-regulated by ppGpp and co-expressed[5, 46-49] under both nutrient limitation and Cm inhibition. **(B)** Plot of tRNA/cell against rRNA/cell upon nutrient limitation[5] show that these parameters are proportional to each other. The slope shows that there are ~9 tRNA per ribosome.
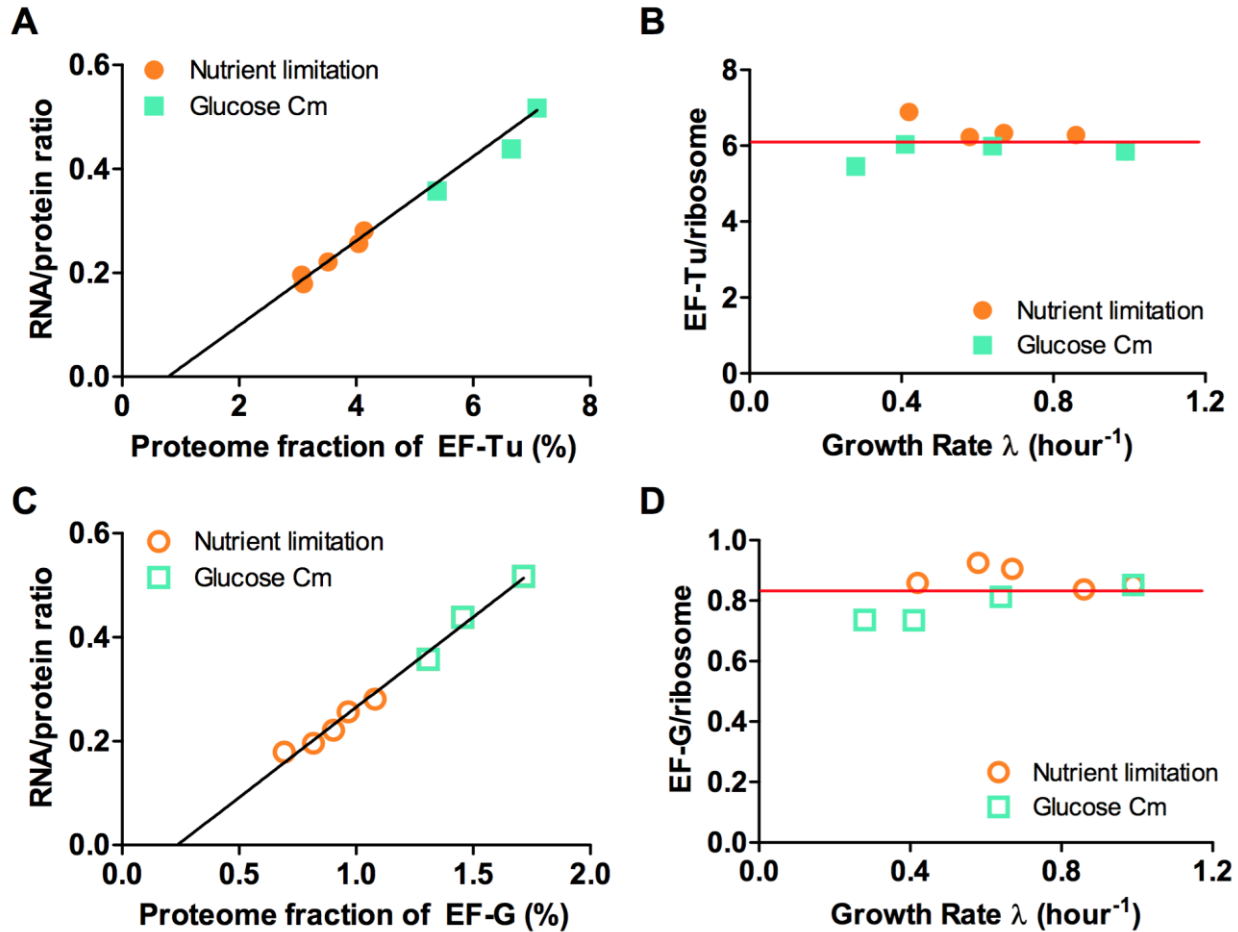
Supplementary Figure 16 The abundances of ribosome, EF-Tu, and EF-G for cells growing under nutrient limitation and chloramphenicol inhibition. The relative abundances of EF-Tu and EF-G for NCM3722 cells under nutrient limitation and Cm inhibition have been determined by Hui *et al*[14] using quantitative mass spectroscopy. Nutrient limitation series in Hui *et a*l was achieved by titrating the lactose uptake using strain NQ381 (an NCM3722 derived strain whose lactose transporter LacY was under the control of a titratable promoter) growing on lactose minimal medium, together with the conditions where wild type NCM3722 strain was grown at lactose minimal medium. The Cm inhibition series (Cm level ranging from 0 to 8μM) in Hui *et al* was performed in glucose minimal medium, which is the same as in this study. The absolute abundances of the proteins, shown as the fraction of total protein content (plotted as the x-coordinate in panels A and C) were obtained by calibrating the result of Hui *et al* with a reference strain (MG1655) for which the abundances of all its individual proteins were already known from a recent ribosome profiling experiment[22]. In Hui *et al*, mass spectroscopy was performed for both the nutrient limitation and Cm inhibition series together with the above-mentioned reference strain, with the latter grown in MOPS glucose minimal medium, the exact same condition as used in Li et al[22] so that the proteome abundance information from Li et al[22] can be directly used as calibration. These absolute proteome abundances of EF-Tu and EF-G

obtained in this way are plotted against the RNA/protein ratio for the same strains measured under the same growth conditions. For each of the growth conditions reported in panels A and C, the number of EF-Tu and EF-G were computed from their absolute abundance using the molecular weights (43,238 for EF-Tu, 77,581 for EF-G). From the RNA/protein ratio, the number of ribosomes was computed using the molecular weight of 1,479,384 for rRNA. Then the ratio of the number of EF-Tu/ribosome is plotted in panel B and the number of EF-G/ribosome is plotted in panel D. We obtained an average of 6.1 EF-Tu per ribosome and 0.83 EF-G per ribosome, shown as the red horizontal line in panel B and D, respectively.

A

Leu1

Glucose   Glucose   0.075%
          8 μM Cm   Mannose

Base treatment

Charged

Uncharged

Glucose   0.075%   Glucose
           Mannose   8 μM Cm

Base treatment

Charged

Uncharged

Glu2

B Glu2

C Leu1

D Leu3

E Arg2

**F** Asp1

G Gly3
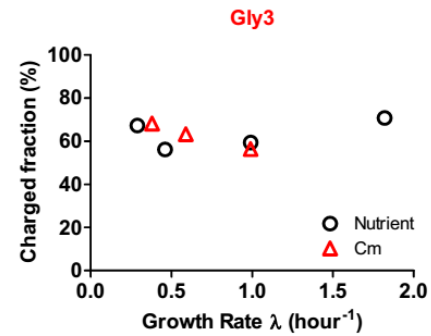
Supplementary Figure 17 Charged fraction of tRNA under nutrient limitation and Cm inhibition. In Supplementary Figure 15, we showed that the level of tRNA and rRNA (they are referred together as "stable RNA") are proportional with each other. Actually what we need to confirm is whether charged tRNA are also proportional to rRNA. The charged fractions of six tRNA species are measured by northern blotting. **A.** Two typical northern blotting images for Glu2 and Leu1. In a typical image of tRNA northern blotting, there are two bands which are resolved, one is charged tRNA (upper one), the other is uncharged tRNA (lower one). By using base (Tris-HCl) treatment, all the charged tRNA becomes uncharged tRNA, which can be used as a reference band. By comparing the intensity of charged fraction and uncharged fraction of tRNA, we got the charged ratio of six individual tRNA species at both nutrient limitation and Cm inhibition. For nutrient limitation, we selected four conditions (from fast growth to slow growth), RDM +glucose, glucose, acetate, 0.075% Mannose. For Cm, we selected glucose+4 μM Cm, and glucose+8 μM Cm. **B. Glu2; C. Leu1; D. Leu3; E. Arg2; F. Asp1; G. Gly3.** Data of every condition was repeated for three times and the deviation was within 10%. For all these six tRNA species, charged tRNA keeps nearly constant for all the growth conditions.
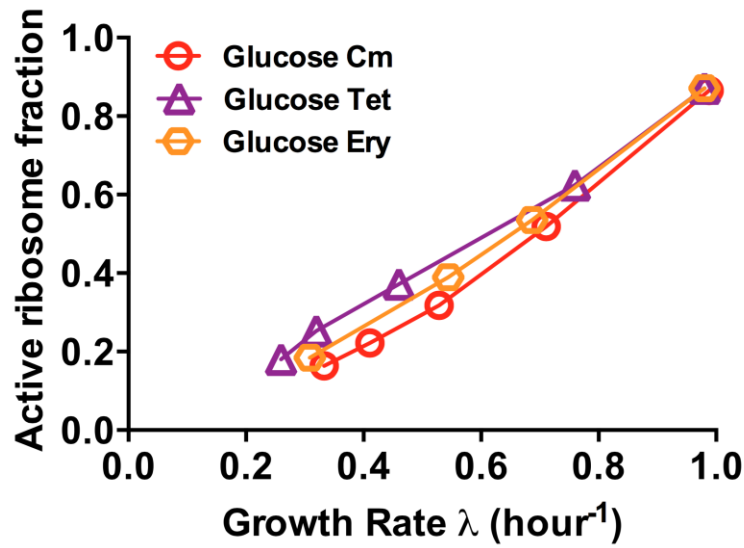
Supplementary Figure 18 Fraction of active ribosome equivalent (f_{active}) under various translation inhibiting antibiotics. Fraction of active ribosomes equivalent for cells under sub-lethal doses of Tetracyline (Tet) and Erythromycin (Ery) were calculated from the translational elongation rate (Supplementary Figure 13A and B) and RNA/protein ratio (Supplementary Figure 14A, B) according to Eq. [N1.5]. Cm, Tet and Ery are seen to cause similar reduction of active ribosome fraction.
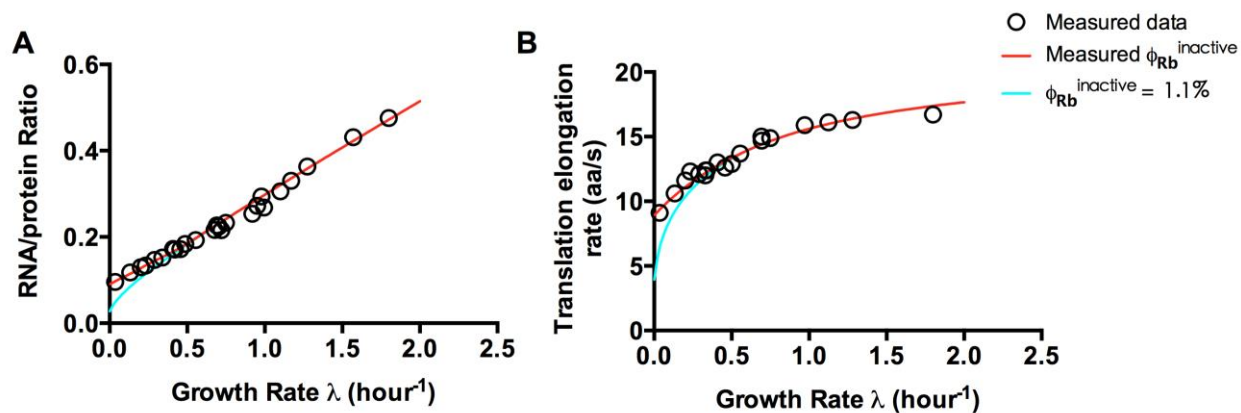
Supplementary Figure 19 Prediction of the crowding theory. The predicted dependence of the RNA-protein ratio $r(\lambda)$ and the translational elongation rate $k(\lambda)$, obtained from solving Eq. [N4.1] and [N4.2] respectively, is plotted as the lines in panels A and B respectively, with the cyan line being the result for a fixed inactive ribosome fraction (1.1% of the proteome) and the red line being results generated from the measured (growth-rate dependent) inactive ribosome fraction shown in Fig. 3D. The plots show that the crowding theory with a constant fraction of inactive ribosomes (cyan lines) is grossly off in the slow growth regime. However, the theory accurately captures the data (red line) when the measured inactive ribosome fraction is used. See Supp Note 4 for details.
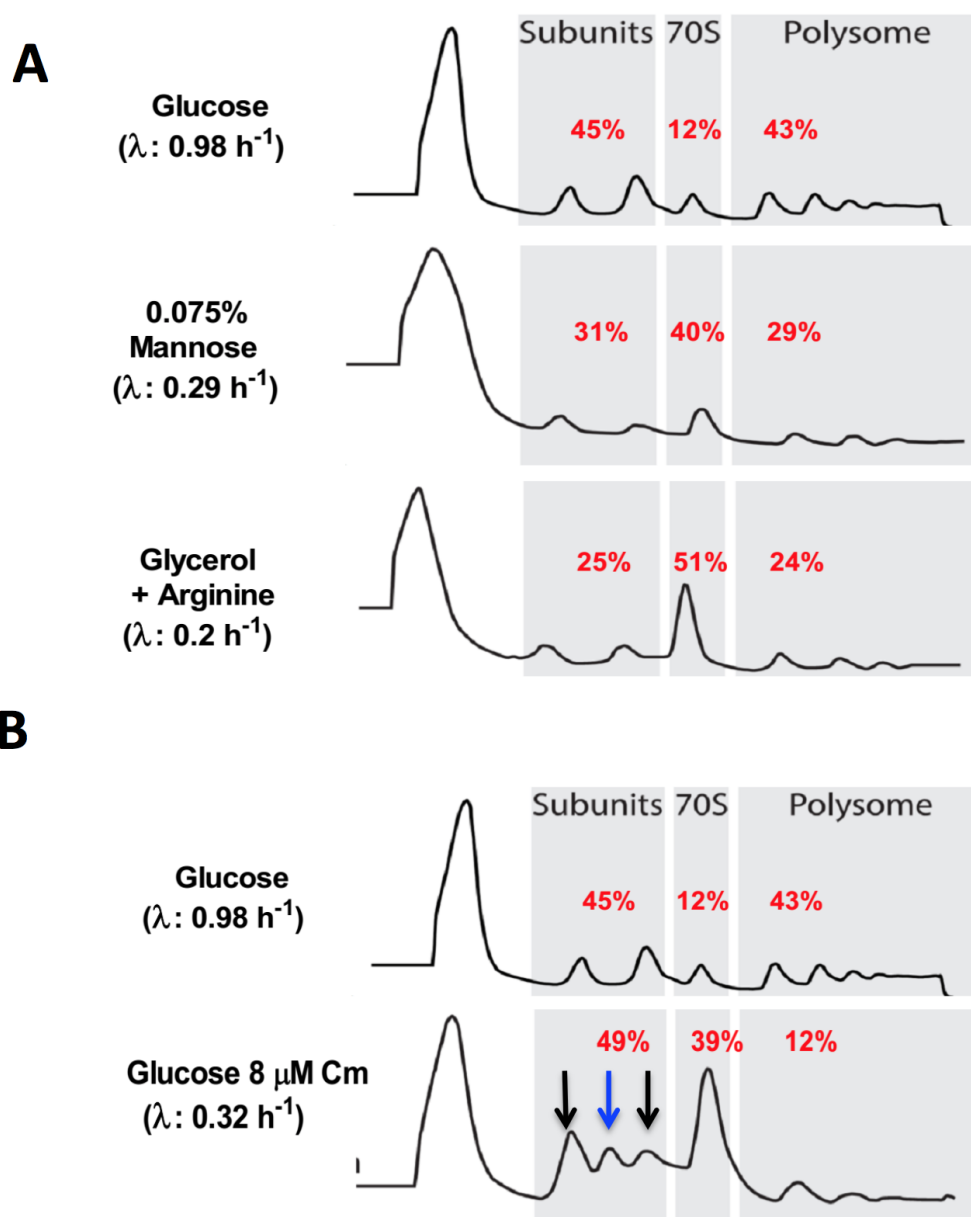
Supplementary Figure 20 Polysome profiling of *E. coli* cells under four growth conditions.
Three major ribosome populations including polysome, 70S monosome, and subunits (both 30S
and 50S) are presented in polysome profiling data. The red number denotes the relative fraction
of each of the three ribosomes populations in every fixed condition. The absolute abundance (size
of the peak) of the same ribosome populations among different nutrient conditions (the same
column) cannot be directly compared due to different loading total RNA concentration. (A) Three
different nutrient conditions. (B) Glucose condition with or without Cm. In the subunit band,
there is an extra peak (blue arrow) occurring between 30S and 50S subunits (black color).
Polysome profiling results have been repeated for three times with one typical figure shown
above.

Supplementary Reference:

1   Maaløe, O. Regulation of the protein-synthesizing machinery - ribosomes, tRNA, factors, and so on. *Biological Regulation and Development, ed Goldberger RF* (Plenum, New York). (1979).

2   Neidhardt, F. C. & Magasanik, B. Studies on the role of ribonucleic acid in the growth of bacteria. *Biochim Biophys Acta* **42**, 99-116, (1960).

3   Churchward, G., Bremer, H. & Young, R. Macromolecular composition of bacteria. *J Theor Biol* **94**, 651-670, (1982).

4   Schaechter, M., Maaloe, O. & Kjeldgaard, N. O. Dependency on medium and temperature of cell size and chemical composition during balanced grown of Salmonella typhimurium. *J Gen Microbiol* **19**, 592-606, (1958).

5   Bremer, H. & Dennis, P. P. Modulation of chemical composition and other parameters of the cell at different exponential growth rates. *Escherichia coli and Salmonella, ed Neidhardt FC (Am Soc Microbiol, Washington,DC), 2nd Ed*, 1553–1569, (1996).

6   Scott, M., Gunderson, C. W., Mateescu, E. M., Zhang, Z. & Hwa, T. Interdependence of cell growth and gene expression: origins and consequences. *Science* **330**, 1099-1102, (2010).

7   Nath, K. & Koch, A. L. Protein degradation in Escherichia coli. I. Measurement of rapidly and slowly decaying components. *J Biol Chem* **245**, 2889-2900, (1970).

8   Klumpp, S., Scott, M., Pedersen, S. & Hwa, T. Molecular crowding limits translation and cell growth. *Proc Natl Acad Sci U S A* **110**, 16754-16759, (2013).

9   Harvey, R. J. & Koch, A. L. How partially inhibitory concentrations of chloramphenicol affect the growth of Escherichia coli. *Antimicrob Agents Chemother* **18**, 323-337, (1980).

10   Liang, S. T., Ehrenberg, M., Dennis, P. & Bremer, H. Decay of rplN and lacZ mRNA in Escherichia coli. *J Mol Biol* **288**, 521-538, (1999).

11   Uemura, S. *et al.* Real-time tRNA transit on single translating ribosomes at codon resolution. *Nature* **464**, 1012-1017, (2010).

12   Pestka, S. Binding of [14C]erythromycin to Escherichia coli ribosomes. *Antimicrob Agents Chemother* **6**, 474-478, (1974).

13   Janssen, B. D., Diner, E. J. & Hayes, C. S. Analysis of aminoacyl- and peptidyl-tRNAs by gel electrophoresis. *Methods Mol Biol* **905**, 291-309, (2012).

14   Hui, S. *et al.* Quantitative proteomic analysis reveals a simple strategy of global resource allocation in bacteria. *Mol Syst Biol* **11**, 784, (2015).

15   Basan, M. *et al.* Inflating bacterial cells by increased protein synthesis. *Mol Syst Biol* **11**, 836, (2015).

16   Cayley, S., Lewis, B. A., Guttman, H. J. & Record, M. T., Jr. Characterization of the cytoplasm of Escherichia coli K-12 as a function of external osmolarity. Implications for protein-DNA interactions in vivo. *J Mol Biol* **222**, 281-300, (1991).

17   Dong, H., Nilsson, L. & Kurland, C. G. Co-variation of tRNA abundance and codon usage in Escherichia coli at different growth rates. *J Mol Biol* **260**, 649-663, (1996).

18   Liang, S. T., Xu, Y. C., Dennis, P. & Bremer, H. mRNA composition and control of bacterial gene expression. *J Bacteriol* **182**, 3037-3044, (2000).

19   Hayes, C. S. & Sauer, R. T. Cleavage of the A site mRNA codon during ribosome pausing provides a

mechanism for translational quality control. *Mol Cell* **12**, 903-911, (2003).

20   Keiler, K. C. Mechanisms of ribosome rescue in bacteria. *Nat Rev Microbiol* **13**, 285-297, (2015).

21   Steinsiek, S. & Bettenbrock, K. Glucose transport in Escherichia coli mutant strains with defects in sugar transport systems. *J Bacteriol* **194**, 5897-5908, (2012).

22   Li, G. W., Burkhardt, D., Gross, C. & Weissman, J. S. Quantifying absolute protein synthesis rates reveals principles underlying allocation of cellular resources. *Cell* **157**, 624-635, (2014).

23   Bennett, P. M. & Maaloe, O. The effects of fusidic acid on growth, ribosome synthesis and RNA metabolism in Escherichia coli. *J Mol Biol* **90**, 541-561, (1974).

24   Schleif, R., Hess, W., Finkelstein, S. & Ellis, D. Induction kinetics of the L-arabinose operon of Escherichia coli. *J Bacteriol* **115**, 9-14, (1973).

25   Langley, K. E., Villarejo, M. R., Fowler, A. V., Zamenhof, P. J. & Zabin, I. Molecular basis of beta-galactosidase alpha-complementation. *Proc Natl Acad Sci U S A* **72**, 1254-1257, (1975).

26   Ruusala, T., Andersson, D., Ehrenberg, M. & Kurland, C. G. Hyper-accurate ribosomes inhibit growth. *EMBO J* **3**, 2575-2580, (1984).

27   Zengel, J. M., Young, R., Dennis, P. P. & Nomura, M. Role of ribosomal protein S12 in peptide chain elongation: analysis of pleiotropic, streptomycin-resistant mutants of Escherichia coli. *J Bacteriol* **129**, 1320-1329, (1977).

28   Pedersen, S. Escherichia coli ribosomes translate in vivo with variable rate. *EMBO J* **3**, 2895-2898, (1984).

29   Dalbow, D. G. & Young, R. Synthesis time of beta-galactosidase in Escherichia coli B/r as a function of growth rate. *Biochem J* **150**, 13-20, (1975).

30   Young, R. & Bremer, H. Polypeptide-chain-elongation rate in Escherichia coli B/r as a function of growth rate. *Biochem J* **160**, 185-194, (1976).

31   Withey, J. H. & Friedman, D. I. The biological roles of trans-translation. *Curr Opin Microbiol* **5**, 154-159, (2002).

32   Handa, Y., Inaho, N. & Nameki, N. YaeJ is a novel ribosome-associated protein in Escherichia coli that can hydrolyze peptidyl-tRNA on stalled ribosomes. *Nucleic Acids Res* **39**, 1739-1748, (2011).

33   Shimizu, Y. Biochemical aspects of bacterial strategies for handling the incomplete translation processes. *Front Microbiol* **5**, 170, (2014).

34   Giudice, E. & Gillet, R. The task force that rescues stalled ribosomes in bacteria. *Trends Biochem Sci* **38**, 403-411, (2013).

35   Moore, S. D. & Sauer, R. T. Ribosome rescue: tmRNA tagging activity and capacity in Escherichia coli. *Mol Microbiol* **58**, 456-466, (2005).

36   Farrell, C. M., Grossman, A. D. & Sauer, R. T. Cytoplasmic degradation of ssrA-tagged proteins. *Mol Microbiol* **57**, 1750-1761, (2005).

37   Pato, M. L., Bennett, P. M. & von Meyenburg, K. Messenger ribonucleic acid synthesis and degradation in Escherichia coli during inhibition of translation. *J Bacteriol* **116**, 710-718, (1973).

38   Siibak, T. *et al.* Erythromycin- and chloramphenicol-induced ribosomal assembly defects are secondary effects of protein synthesis inhibition. *Antimicrob Agents Chemother* **53**, 563-571, (2009).

39   Holmes, I. A. & Wild, D. G. Inhibition of the growth of Escherichia coli by chlortetracycline. *Biochem J* **104**, 679-685, (1967).

40   Chopra, I. & Howe, T. G. Bacterial resistance to the tetracyclines. *Microbiol Rev* **42**, 707-724, (1978).

41   Muto, A., Kimura, A. & Osawa, S. Effects of some antibiotics on the stringent control of RNA synthesis in Escherichia coli. *Mol Gen Genet* **139**, 321-327, (1975).

42   Schlunzen, F. *et al.* Structural basis for the interaction of antibiotics with the peptidyl transferase centre in eubacteria. *Nature* **413**, 814-821, (2001).

43   Kannan, K. *et al.* The general mode of translation inhibition by macrolide antibiotics. *Proc Natl Acad Sci U S A* **111**, 15958-15963, (2014).

44   Lund, E. & Kjeldgaard, N. O. Metabolism of guanosine tetraphosphate in Escherichia coli. *Eur J Biochem* **28**, 316-326, (1972).

45   Brock, T. D. & Brock, M. L. Similarity in mode of action of chloramphenicol and erythromycin. *Biochim Biophys Acta* **33**, 274-275, (1959).

46   Ryals, J., Little, R. & Bremer, H. Control of rRNA and tRNA syntheses in Escherichia coli by guanosine tetraphosphate. *J Bacteriol* **151**, 1261-1268, (1982).

47   Jinks-Robertson, S., Gourse, R. L. & Nomura, M. Expression of rRNA and tRNA genes in Escherichia coli: evidence for feedback regulation by products of rRNA operons. *Cell* **33**, 865-876, (1983).

48   Shen, V. & Bremer, H. Rate of ribosomal ribonucleic acid chain elongation in Escherichia coli B/r during chloramphenicol treatment. *J Bacteriol* **130**, 1109-1116, (1977).

49   Shen, V. & Bremer, H. Chloramphenicol-induced changes in the synthesis of ribosomal, transfer, and messenger ribonucleic acids in Escherichia coli B/r. *J Bacteriol* **130**, 1098-1108, (1977).